

# Surgical tool classification and localization: results and methods from the MICCAI 2022 SurgToolLoc challenge

Aneeq Zia<sup>1</sup>, Kiran Bhattacharyya<sup>1</sup>, Xi Liu<sup>1</sup>, Max Berniker<sup>1</sup>, Ziheng Wang<sup>1</sup>, Rogerio Nespolo<sup>1</sup>, Satoshi Kondo<sup>2</sup>, Satoshi Kasai<sup>3</sup>, Kousuke Hirasawa<sup>4</sup>, Bo Liu<sup>5</sup>, David Austin<sup>5</sup>, Yiheng Wang<sup>5</sup>, Michal Futrega<sup>5</sup>, Jean-Francois Puget<sup>5</sup>, Zhenqiang Li<sup>6</sup>, Yoichi Sato<sup>6</sup>, Ryo Fujii<sup>7</sup>, Ryo Hachiuma<sup>7</sup>, Mana Masuda<sup>7</sup>, Hideo Saito<sup>7</sup>, An Wang<sup>8</sup>, Mengya Xu<sup>10, 11</sup>, Mobarakol Islam<sup>9</sup>, Long Bai<sup>8</sup>, Winnie Pang<sup>10</sup>, Hongliang Ren<sup>8, 10, 11</sup>, Chinedu Nwoye<sup>12,14</sup>, Luca Sestini<sup>12,13</sup>, Nicolas Padoy<sup>12,14</sup>, Maximilian Nielsen<sup>15</sup>, Samuel Schüttler<sup>15</sup>, Thilo Sentker<sup>15</sup>, Hümeýra Hussein<sup>15</sup>, Ivo Baltruschat<sup>15</sup>, Rüdiger Schmitz<sup>15</sup>, René Werner<sup>15</sup>, Aleksandr Matsun<sup>16</sup>, Mugariya Farooq<sup>16</sup>, Numan Saaed<sup>16</sup>, Jose Renato Restom Viera<sup>16</sup>, Mohammad Yaqub<sup>16</sup>, Neil Getty<sup>17,18,19</sup>, Fangfang Xia<sup>17,18,19</sup>, Zixuan Zhao<sup>17,18</sup>, Xiaotian Duan<sup>17,18</sup>, Xing Yao<sup>20</sup>, Ange Lou<sup>20</sup>, Hao Yang<sup>20</sup>, Jintong Han<sup>20</sup>, Jack Noble<sup>20</sup>, Jie Ying Wu<sup>20</sup>, Tamer Abdalbaki Alshirbaji<sup>21,22</sup>, Nour Aldeen Jalal<sup>21,21</sup>, Herag Arabian<sup>21</sup>, Ning Ding<sup>21</sup>, Knut Moeller<sup>21,23,24</sup>, Weiliang Chen<sup>25</sup>, Quan He<sup>26</sup>, Lena Maier-Hein<sup>28</sup>, Danail Stoyanov<sup>27</sup>, Stefanie Speidel<sup>29</sup>, and Anthony Jarc<sup>1</sup>

<sup>1</sup>Intuitive Surgical, Inc., <sup>2</sup>Muroran Institute of Technology, <sup>3</sup>Niigata University of Health and Welfare, <sup>4</sup>Konica Minolta, Inc., <sup>5</sup>NVIDIA, Inc., <sup>6</sup>University of Tokyo, <sup>7</sup>Keio University, <sup>8</sup>Shun Hing Institute of Advanced Engineering, <sup>9</sup>Wellcome EPSRC Centre for Interventional and Surgical Sciences, <sup>10</sup>NUS, <sup>11</sup>NUSRI SZ, <sup>12</sup>University of Strasbourg, <sup>13</sup>Politecnico di Milano, <sup>14</sup>IHU Strasbourg, <sup>15</sup>University Medical Center Hambrug-Eppendorf, <sup>16</sup>Bin Zayed University of Artificial Intelligence, <sup>17</sup>Argonne National Laboratory, <sup>18</sup>University of Chicago, <sup>19</sup>University of Illinois at Chicago, <sup>20</sup>Vanderbilt University, <sup>21</sup>Furtwangen University, <sup>22</sup>University of Leipzig, <sup>23</sup>University of Canterbury, <sup>24</sup>University of Freiburg, <sup>25</sup>South China University of China, <sup>26</sup>Hikvision Research Institute, <sup>27</sup>University College London, <sup>28</sup>German Cancer Research Center (DKFZ), <sup>29</sup>National Center for Tumor Diseases (NCT)

## Abstract

The ability to automatically detect and track surgical instruments in endoscopic videos can enable transformational interventions. Assessing surgical performance and efficiency, identifying skilled tool use and choreography, and planning operational and logistical aspects of OR resources are just a few of the applications that could benefit. Unfortunately, obtaining the annotations needed to train machine learning models to identify and localize surgical tools is a difficult task. Annotating bounding boxes frame-by-frame is tedious and time-consuming, yet large amounts of data with a wide variety of surgical tools and surgeries must be captured for robust training. Moreover, ongoing annotator training is needed to stay up to date with surgical instrument innovation. In robotic-assisted surgery, however, potentially informative data like timestamps of instrument installation and removal can be programmatically harvested. The ability to rely on tool installation data alone would significantly reduce the workload to train robust tool-tracking models. With this motivation in mind we invited the surgical data science community to participate in the challenge, SurgToolLoc 2022. The goal was to leverage tool presence data as weak labels for machine learning models trained to detect tools and localize them in video frames with bounding boxes. We present the results of this challenge along with many of the team’s efforts. We conclude by discussing these results in the broader context of machine learning and surgical data science. The training data used for this challenge consisting of 24,695 video clips with tool presence labels is also being released publicly and can be accessed at <https://console.cloud.google.com/storage/browser/isi-surgtoolloc-2022>.

# 1 Introduction

Robotic-assisted (RA) surgeries become more prevalent with each passing year [1, 2]. Clinical results from RA procedures can be used to derive valuable insights to make surgery safer. Importantly, RA surgeries also generate rich streams of data, e.g. video recordings, tool kinematics, and events gathered from the robotic system, that lend themselves to quantitative analyses. Pursuits such as the quantification of surgical performance, autonomous analysis of procedures, surgical skill evaluation, AI-guided surgical planning, and surgical data science, in general, all rely on this data [3–12]. However, despite collecting large amounts of it, annotating it to provide meaningful context remains a major bottleneck in the field.

Acquiring annotations for surgical data is particularly challenging as it requires personnel with in-depth domain knowledge. What’s more, relying solely on human annotators is costly, time-consuming, and subject to inter-rater variability. Yet RA procedures generate numerous, potentially instructive, labels that can be harvested automatically from the system. For example, each instrument install (or uninstall) elicits events that record the tool type and the install (uninstall) time. Similarly, commands to these tools, such as the use of energy, elicit related events. While events such as this are informative, they are noisy and may not be representative of the tools visible in the surgical field, let alone their spatial locations. Machine learning techniques that could reliably exploit these events as noisy, weak labels for training would prove extremely valuable. While algorithms for this class of problem exist, there is a real need for advancements in their accuracy and robustness.

Machine learning (ML) challenges –also known as competitions– have become an integral part of many top computer vision and machine learning conferences [13]. These competitions aim to address specific problems within various fields where the organizers provide the required data set and/or labels. In the surgical domain specifically, EndoVis<sup>1</sup> is an annual challenge held at the international Conference on Medical Image Computing and Computer Assisted Intervention MICCAI<sup>2</sup>. This challenge contains multiple sub-challenges targeting problems like tissue and instrument tracking and segmentation, 3D scene reconstruction, action recognition, and surgical skills assessment [14–18]. Following suit, our team organized the SurgToolLoc 2022 challenge.

SurgToolLoc 2022 was held as a sub-challenge at EndoVis 2022. The aim of this sub-challenge was to address the problem of weakly supervised learning of surgical tool localization in RA procedures, while also fostering work on practical deep-learning solutions. For this challenge, we provided participating teams with an extensive set of endoscopic video data consisting of 24,695 video clips. Together with the videos, the teams received noisy annotations for the surgical tools present in each video frame. The ultimate goal of this challenge was to utilize automatically extracted tool labels to build models that can classify and localize surgical instrumentation in a hidden test set. Here we present an overview of the challenge, most of the participating teams submitted solution methods, and the results in general.

Lastly, to encourage the surgical data science community to continue working on similar problems, the training data used in this challenge will be released publicly as part of this publication. To the best of our knowledge, this is the largest publicly available surgical data set to date. It is our firm hope that this ongoing challenge and the accompanying data sets become touchstones for the broader field of surgical data science.

## 2 SurgToolLoc 2022 Challenge Description

### 2.1 Challenge Overview

The sub-challenge was arranged as part of the Endoscopic Vision Challenge at MICCAI 2022. The challenge had two separate categories open to the participating teams (Figure 1). Category 1 focused on identifying the presence of surgical tools in video frames, while Category 2 challenge was designed in order to identify both those tools present and their locations in the corresponding video frames.

Both categories required the development of weakly supervised algorithms. The first category relied on supervised learning for object detection with weak/noisy labels. The second category required weakly supervised object detection and localization with the same labels. Teams were allowed to participate in either challenge or both.

---

<sup>1</sup><https://endovis.grand-challenge.org/>

<sup>2</sup><https://conferences.miccai.org/2022>

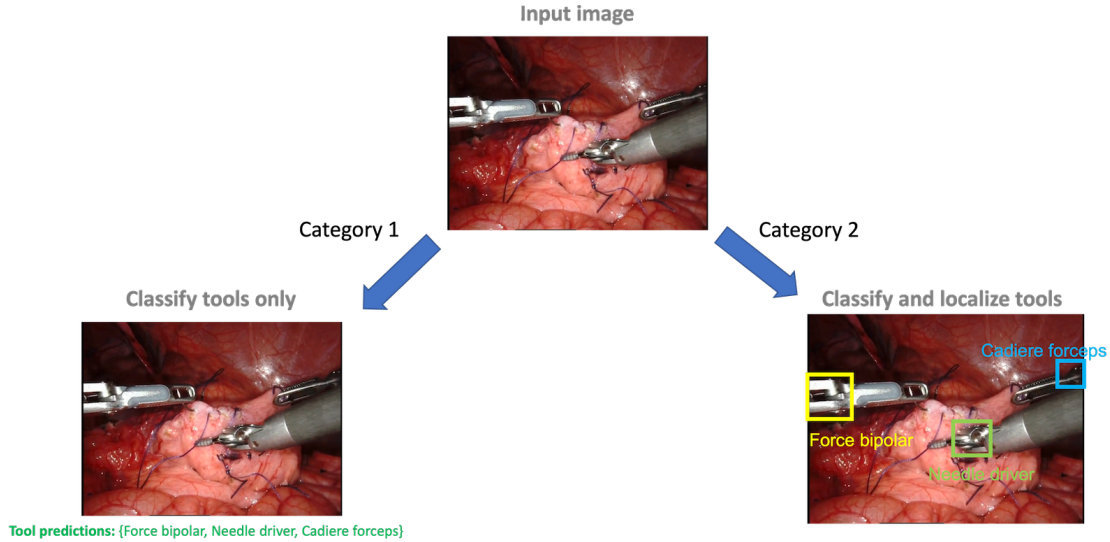


Figure 1: Overview of challenge categories 1 and 2

## 2.2 Category 1: Surgical Tool Classification

This category required the teams to submit a model that could classify all the tools present (up to 3 surgical instruments) within 30-second video clips. This required the teams to train a multi-label model to classify the 14 possible tools. A data set of 24,695 video clips was provided for training. The accompanying labels indicated which robotic tools were present in each clip. For technical reasons, a portion of the labels was missing or incorrectly assigned.

Submissions were evaluated on a hidden test data set of surgical videos through the Grand Challenge’s automated docker submission and evaluation system. Teams were ranked by their model’s average F1 score across all classes.

## 2.3 Category 2: Surgical Tool Classification & Detection

This category required the models to perform the same classification problem as before while also localizing the identified tools with bounding boxes for each frame. As in Category 1, the models localized the tools present within a set of 30-second video clips.

## 2.4 Data Collection

Video and system data were harvested from surgical training exercises performed on the da Vinci robotic system. During these exercises, surgical trainees (and some experts) performed a series of standardized activities on porcine tissue, such as dissecting, suturing, and cauterizing. The captured video displays the trainee’s view from the surgeon’s console, although it is only one of the two video streams from the stereoscopic imaging system. System data that indicate which tools are present was also collected.

The training exercises that generated the data were performed on two distinct animal modalities, either an anesthetized living pig, or using organs harvested from a pig. This distinction leads to differences in the general appearance of the resulting video frames, and those of the former modality are generally redder in tone. The anatomy present in the videos was not relevant to this challenge. However, across all the videos, 14 tools were installed and visible. They were: needle driver, cadiere forceps, prograsp forceps, monopolar curved scissors, bipolar forceps, stapler, force bipolar, vessel sealer, permanent cautery hook/spatula, clip applier, tip-up fenestrated grasper, suction irrigator, bipolar dissector, and grasping retractor.

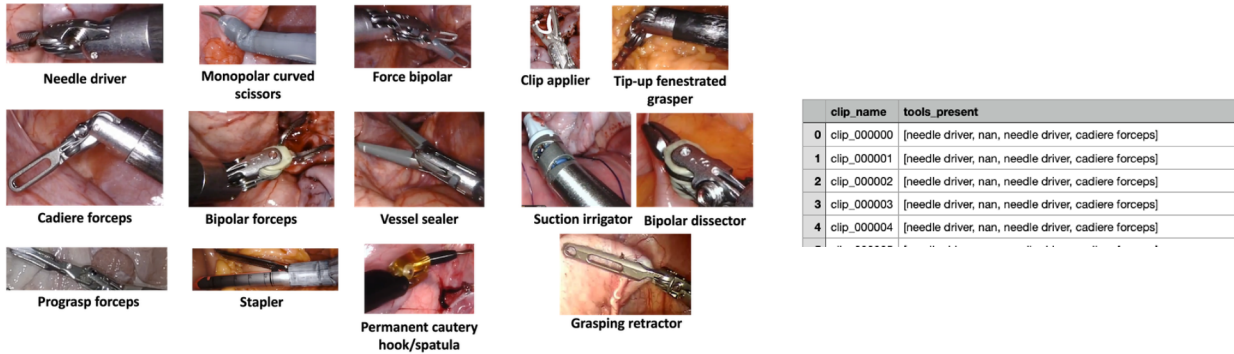


Figure 2: Sample frames with presence labels (left) and a snapshot of the labels CSV file (right)

## 2.5 Training Data

From the data collected, 24,695 video clips from a set of 11 unique training exercises were made available for training purposes. Each clip was 30 seconds long and captured at 60 FPS with a resolution of 720p (1280 x 720) from one channel of the binocular endoscope (Figure 2). For the extent of each clip, there were up to three robotic surgical tools simultaneously installed within the surgical field. For each video clip within the training set, we provided the corresponding tool presence labels that indicated which robotic tools are installed. Since the tools are installed for the entire duration of each video clip, only one label per video clip was provided. Notably, for some clips, or portions of clips, tools were obscured or otherwise temporarily not visible. Moreover, the instrument distribution among the data was highly imbalanced. As such, the tool presence labels were noisy indicators of the presence of a surgical instrument in the video frames. The teams were also allowed to pre-train their models on publicly available surgical datasets such as Cholec80 [19] and M2CAI [20], and comprehensive datasets such as ImageNet [21].

Presence labels were a list of four strings corresponding to the tools present in the robot’s four arms [USM1, USM2, USM3, USM4], e.g. [‘cadiere forceps’, ‘nan’, ‘force bipolar’, ‘grasping retractor’], where the arm with the camera installed is labeled as “nan.” The four arms are usually (though not necessarily) installed from left to right (i.e. USM1 is the leftmost arm, and USM4 is the rightmost arm). Figure 2 shows an example of the .csv file with the presence labels. This training data set has also been released publicly and can be accessed at <https://console.cloud.google.com/storage/browser/isi-surgtoolloc-2022>.

## 2.6 Testing Data

The testing dataset consisted of 93 video clips taken from surgical training exercises - similar to the training set-, using the da Vinci robotic system. The length of each video clip was variable-mean(SD), in seconds: 747.31(579.92)-, but had the same resolution and was sub-sampled to 1 frame-per-second (FPS) for inference purposes. The testing dataset had the tool presence labels in the same way as for the training set but also combined with annotated bounding boxes around the instruments. These annotations were generated by a crowd (30) of experienced annotators. Two rounds of annotation reviews were conducted to ensure quality. It is important to note that the clevis of each robotic surgical tool was considered the ground truth for most tools as Figure 3 shows. However, there are following exceptions to this rule: If a tool’s clevis is not well defined or if the tool is especially large and the clevis does not always show in the field of view, then the bounding box includes the surgical tip as well - e.g monocular curve scissor as shown in the purple-colored bounding box on the left of Figure 3. Moreover, using the information available in the UI to make predictions was not allowed. To enforce this, the area comprising the UI interface in the test set was blurred, as seen in Figure 3.

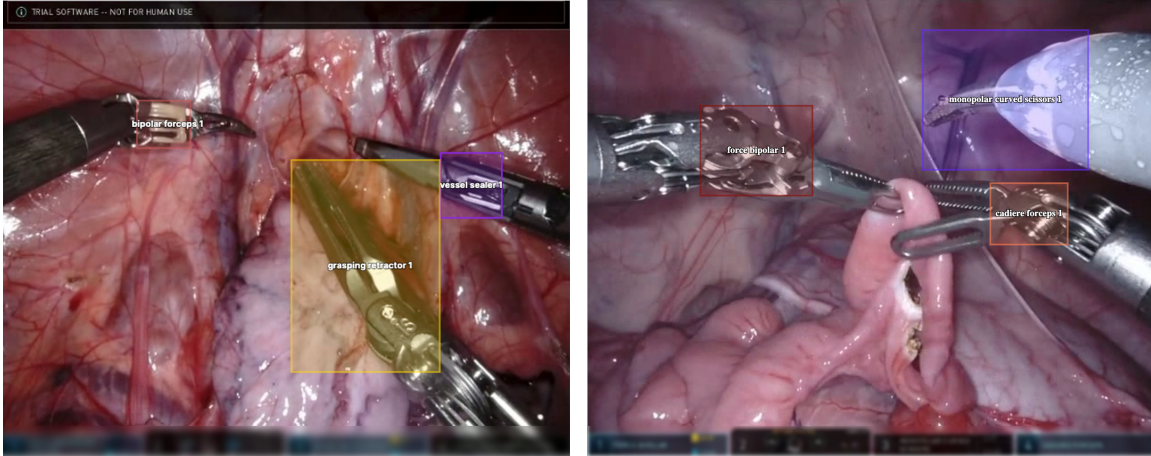


Figure 3: Sample frames with testing labels. The UI interface was blurred to avoid its embedded information (description of the tools) being used for predictions.

## 2.7 Submission Process

The challenge was hosted as a “Type 2 (T2) challenge” on the grand-challenge (GC) platform<sup>3</sup>. T2 challenges on GC allow for the automated submission of containers, while the evaluation process for these submissions is executed via a standardized evaluation protocol to ensure the reproducibility of the algorithm. This modality also allows for each algorithm to be evaluated on a private test dataset that is hidden from the teams.

Each team developed its own algorithm following the guidelines provided by the GC platform<sup>4</sup> and the organizing team of the challenge. Every submitted algorithm was configured to receive as input either a preliminary test dataset containing two videos for debugging purposes or the final test dataset described in 2.6. The algorithm’s output had to follow a standardized file format for each category. For category 1 -surgical tool classification-, the output file had to generate a list of dictionaries containing information on the tools present in each frame of the input video in a boolean format. For category 2 - Surgical tool classification and localization-, the algorithm had to output a dictionary containing the set of tools detected in each frame with its corresponding bounding box cartesian coordinates (x, y). Details on the creation of the algorithms, samples of input data, and the required format for output files were provided to the participating teams<sup>5</sup>.

Following each evaluation, the platform’s embedded leaderboard displayed each team’s submission scores. Then, the teams were asked to submit a final report with their methodology and results when evaluating the algorithm with the hidden test dataset. Each report is reproduced in this paper in section 3.

## 3 Team Submissions

For this challenge, there were a total of 79 teams that had shown interest in participating and downloading the dataset. In the end, there were 17 teams that made full submissions in Category 1 whereas 11 made full submissions for Category 2. All teams that participated in Category 2 also participated in Category 1. A table showing the participating teams is presented below (Table 1), while Table 2 summarizes the methodologies employed by each team. What follows in its section are the methodological details of the participating teams. Please note that these sub-sections were written by the participating teams so a difference in writing style and content will be observed.

<sup>3</sup>grand-challenge.org

<sup>4</sup><https://grand-challenge.org/documentation/algorithms/>

<sup>5</sup><https://surgtoolloc.grand-challenge.org/submission/>

Table 1: Team affiliations and challenge categories.

Team #	Team name	Institution	Country	Category	Report
1	HRL_MV	Hikvision Research Institute	China	1 & 2	Y
2	HKMV	South China University of China	China	1 & 2	Y
3	NVIDIA	NVIDIA	USA	1 & 2	Y
4	ANL-Surg	Argonne National Lab	USA	1 & 2	Y
5	HVRL	Keio University	Japan	1 & 2	Y
6	SK	Muroran Institute of Technology, Niigata University of Health and Welfare, Konica Minolta	Japan	1 & 2	Y
7	TeamZERO	University of West of England Bristol, University of Glasgow, University of Bristol	UK	1 & 2	N
8	VANDY-UISE	Vanderbilt University	USA	1 & 2	Y
9	UKE	University Medical Center Hamburg	Germany	1 only	Y
10	Gatech	Georgia Institute of Technology	USA	1 & 2	N
11	ITeM	Furtwangen University, University of Lipzig	Germany	1 & 2	Y
12	MM	Chinese University of Hong Kong, National University of Singapore, University College London	Hong Kong, Singapore, UK	1 only	Y
13	BioMedIA	Muhammad bin Zayed University of Artificial Intelligence	UAE	1 only	Y
14	WhiteBox	The University of Tokyo	Japan	1 only	Y
15	CAMMA	University of Strasbourg	France	1 only	Y
16	Vision_HK	Tianjin University	China	1 & 2	N
17	lsgroup	Xiamen University	China	1 only	N

### 3.1 Hikvision Research Institute - Team HRL\_MV

Team Member: Quan He

The HRL\_MV team made full use of the characteristics of the video data and adopt an object-tracking scheme with a semantic segmentation network to obtain the pseudo tags of the frames. In particular, an IOU scoring with the dual model cross-validation mechanism was employed to choose more reliable pseudo tags. Using the obtained pseudo tags, a detector was trained and integrated into a pseudo tag using a Kalman filter, iteratively updating the models.

In traditional instrument target detection, the whole object is considered as the ground truth (GT) and included in the detection frame, while in surgical instrument detection, only the clevis is considered as GT. The difficulty is that the appearance of the clevis of different devices is relatively similar. When human eyes distinguish different devices, they are actually mainly distinguished according to the clamps of the devices. To solve this problem, the ROI proposal box output by the RPN network was modified: for the regression head, the proposal box output by RPN was used, while for the classification head, the proposal box was expanded to obtain more information for device classification.

Finally, the integration algorithm was adapted to use the detection frame output from the previous frame for target tracking while combining the results of target detection and target tracking by weighting, which effectively solved the problem of target missing detection.

#### 3.1.1 Method Description

Object Tracking with Cross Supervision:

The HRL\_MV team choose to label the frame sequence of the video by using the target tracking method: The first frame of the video was manually labeled, while automatically labeling the subsequent frames using the target tracking algorithm. However, the tracking process sometimes failed. The team found that this was caused by clevis' small and inconspicuous features, reflection, and other factors. Therefore, a cross-validation method based on segmentation results was proposed.

Siamfc++[22] was chosen for single target tracking (SOT). The advantage of this approach is that the trained SOT model can be used without retraining. Only the first frame of the sequence needed to be labeled so the SOT was able to track the subsequent picture frames effectively. Then, an unet-like segmentation network was trained with the open source data dVRK segmentation dataset, Event-based-2D-tracking-of-articulated-instruments-for-robotic-surgery dataset, EndoVis17 dataset, and EndoVis18 dataset.

The detector was trained with part of pseudo labels and then used to generate new pseudo labels with the tracking output. For frames with an IoU less than the threshold value of 0.2, the generated pseudo label was considered untrustworthy. In this way, a dataset containing about 25000 frames with pseudo labels was obtained.

Roi Expand:

Cascade RCNN [23] was chosen as a target detection model. In the initial test results, although many instruments were successfully detected, they were misclassified. This is because, in traditional instrument

Table 2: Summary of methodologies

Team Name	Architecture	Backbone	Data Pre-processing	Pretrain	Image Augmentation	Use Additional Data	Loss	Output
HKMV SK	Faster-RCNN Multiplicity Fusion	efficient-net-b3 ResNet-50	Resize, crop	Endovis17, Endovis18 Segmentation data	N/A	Bounding box generated from segmentation mask N/A		tool bounding box tool class, tool bounding box
NVIDIA	Hybrid (ConvNext-tiny, EfficientNet-B4, Ensemble), YoloV5		Resize, crop		Yes	Pseudo label and manual bounding box		tool class, tool bounding box
WhiteBox	CNN	ResNet-18	Resize, crop		Yes		Asymmetric Focal Loss binary cross-entropy	tool class
HVRL	Hybrid (Swam Transformer, EfficientNet-V2, ResNeXt)		Resize, crop	ImageNet weights, Instagram weights	Yes		Asymmetric Focal Loss weighted sigmoid cross-entropy	tool class
MM	Hybrid (ResNet50, ViT-Batch16)		Resize		Yes		Asymmetric Focal Loss	tool class
CAMMA	Spatial Attention network (SANet)	ResNet-18	Resize	ImageNet weights	Yes		weighted sigmoid cross-entropy	tool class, attention map
UKE	DINO-based ViT	ViT	Resize	ImageNet weights	Yes		focal loss, box regression loss, objectness loss	tool class, attention map, tool bounding box
BioMedIA	YOLOv5, ConvNext	ResNet 50	Oversampling, UI removal	Choice80, Endovis15, ChoiceSeg8k	Yes	Choice80, Endovis15, ChoiceSeg8k datasets		tool class, tool bounding box
ANL-Surg	Ensemble (YOLOv5, ConvNext); Detectron2		Resize, crop	MaskRCNN weights	-	Segmentation labels from MICCAI17 and MICCAI18	Asymmetric loss binary cross-entropy; softmax cross-entropy	tool class, tool bounding box
VANDY-VISE	Query2Label	ResNet, ViT			-			
ITeM	CNN + Squeeze and Excitation (SE) module	ResNet50		Choice80	-			tool class, tool bounding box

target detection, the whole of the object is considered as GT and included in the detection frame, while in surgical instrument detection, only clevis is considered as GT. Although, the appearance of clevis components of different instruments is relatively similar, and the difference is mainly reflected in the clamp part.

To solve this problem, the ROI proposal box output by the RPN network was modified. For the regression head, the proposal box output by RPN was used, while for the classification head, the proposal box was expanded twice in width and height, respectively, to obtain more information for device classification, as shown in Figure 4.

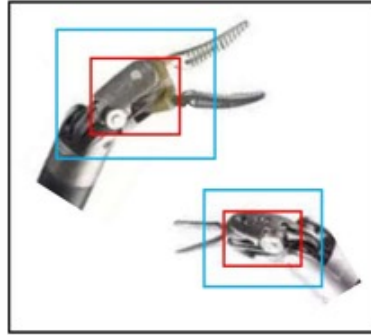


Figure 4: The information required for detection and classification is different. Thus, the ROI proposal box output by RPN network was modified.

Figure 5 shows the feature map extracted from the backbone of the proposed model. In the original model, the instrument cadiere forceps was mistakenly considered prograsp Forceps and tip-up fenestrated Grasper, the thermodynamic values in its characteristic diagram are all concentrated in clevis. With the proposed expanded ROI, the cadiere forceps is correctly classified: in its feature map, there is not only a large thermal value distribution at the clevis but also a large thermal value at the clamp, which helps the model to better classify instruments.

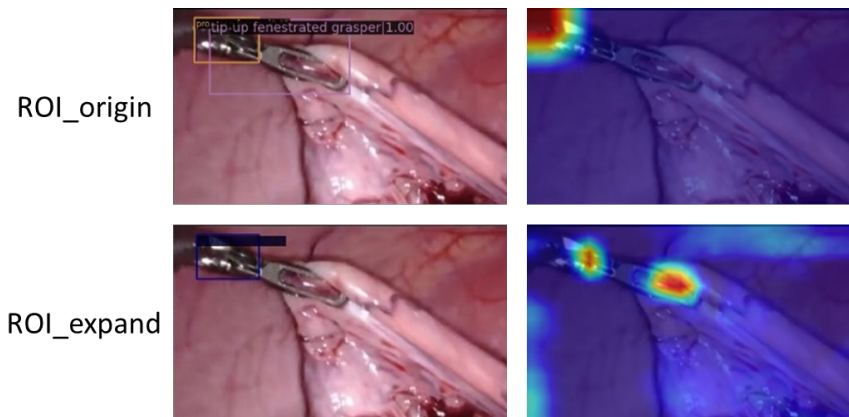


Figure 5: ROI expand makes model identification device

Model ensemble:

The detection frame output from the previous frame algorithm was used for target tracking and integrated into the results of target detection and target tracking via weighting. In this way, as long as the device appears in a certain frame, it can be identified by target tracking in its subsequent frames, solving the problem of target missing detection. The overall framework of our algorithm is shown in Figure 6.

### 3.1.2 Preliminary Performance

A test set was established to verify the performance of the detector to evaluate whether more data is needed. The test set was determined by manual review to include each sample category. *Roundn* means nth times



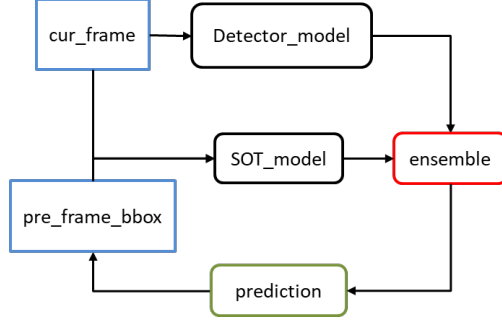


Figure 6: model ensemble

object tracking with the cross supervision method was used to get more data (see Table 3).

Table 3: Object tracking with the Cross Supervision method was used to get more data.

Method	Round1	Round2	Round3	Round4
mean mAP	0.164	0.347	0.489	0.491

By the fourth round, performance has improved slightly. Then, these data were used for the next experiment. The entire dataset was then divided into a training set and test set (7:3) to verify what strategies could be taken to enhance the performance of the model (table 4).

Table 4: Model Results

Method	mean mAP
Base	+0.489
+ swin pre-trained	+0.052
+ roi expand 2	+0.063
+ ChannelShuffle-RGNShift	+0.021
+Fog-Blur-Noise	+0.048
+ focalloss	+0.002
+cbam	+0.033
+DetecoRS pre-trained	+0.059
swin pre-trained + roi expand 2 + Fog-Blur-Noise + ChannelShuffle-RGBShift	+0.109
detectors pre trained + roi expand 2 + Fog-Blur-Noise + ChannelShuffle-RGBShift	+0.111

The mentioned strategies can improve the performance of the model on the current test set; by adopting the ROI expand method, the overall performance was improved by 0.063. Then, the last two models in Table 4 were selected as the models for the ensemble. On the Surgical tool localization Leaderboard, the effectiveness of the ensemble scheme was confirmed: the single model reached a score of 0.3985 on the final test set, while the ensemble model reached a score of 0.4077 and ranked first. Since the detector can classify the target, it was also joined with the Surgical tool detection Tasks. However, on the Surgical tool detection Leaderboard, The performance of the ensemble model deteriorated when compared to that of the single model, with the former score being 0.7485 and the latter being 0.7341.

### 3.2 South China University of China - Team HKMV

Team Member: Weiliang Chen

### 3.2.1 Method Description

In order to obtain an object detection model that can effectively locate surgical tools, the key point is how to build a well-labeled training dataset at a low cost. In this method, two public datasets-endovis17 [24] and endovis18 [25]- were used as the primary training dataset. The clevis part in the mask label of the dataset was converted into a bounding box and then used to train an object detection model. This model was then used to infer the images of the competition dataset and then adjust the predicted bounding box slightly. After repeating several operations, a large-scale training dataset can be obtained.

In terms of the model, a two-stage object detection model was built based on Faster R-CNN. EfficientNet-b3 was chosen here, which takes into account both performance and speed, as the backbone to extract image features and add FPN structure to further optimize the feature map.

Dataset:

Two public datasets endovis17 and endovis18 were used to assist us to obtain a primary training dataset. These two data sets provide mask annotations, as shown in Figure 7.

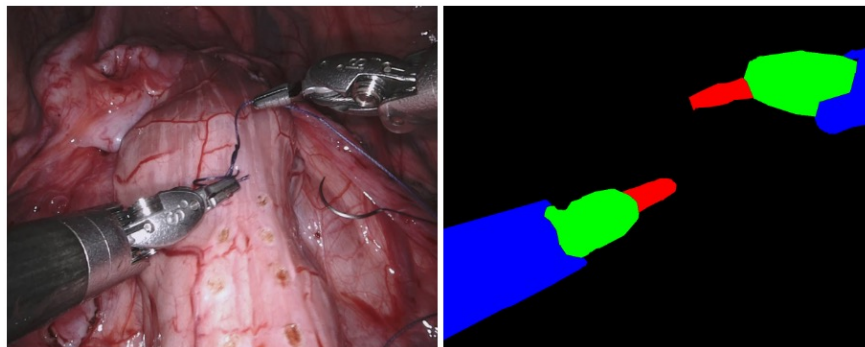


Figure 7: Primary training dataset

The clevis part in the mask label of the dataset was converted into a bounding box label and used as the primary training dataset. Since endovis17 and endovis18 do not include all 14 surgical tools, part of the data was added to the training dataset to ensure that the dataset contains all 14 surgical tools. The final set contained 5212 images.

Surgical Tool Localization Algorithm:

- A Faster R-CNN object detection model was trained on the primary training dataset.
- EfficientNet-b3, which takes into account both performance and speed, was chosen as the backbone to extract image features and add FPN structure to further optimize the feature map.
- According to the size of the clevis of surgical tools in the training dataset, four layers of feature maps were included in the model, which were downsampled 8, 16, 32, and 64 times respectively.

Dataset Expansion and Adjustment:

In order to increase the size of the dataset, the trained model was used to infer the images of the competition dataset, adding these to the training dataset. A score threshold of 0.7 was employed to filter out the poor bounding box. After several operations, the dataset was expanded to 11035 images. The dataset expansion flow diagram of the algorithm is described in Figure 9.

### 3.2.2 Preliminary Performance

For the preliminary experiments, 25% of the dataset was used as the validation dataset, and only well-labeled images were used in order to accurately evaluate our algorithm. The model structure of EfficientNet-b3 was chosen as the backbone, downsampling 8, 16, 32, and 64 times the feature map. During preliminary experiments on this validation dataset, the model was able to reach a mean mAP of 0.452.

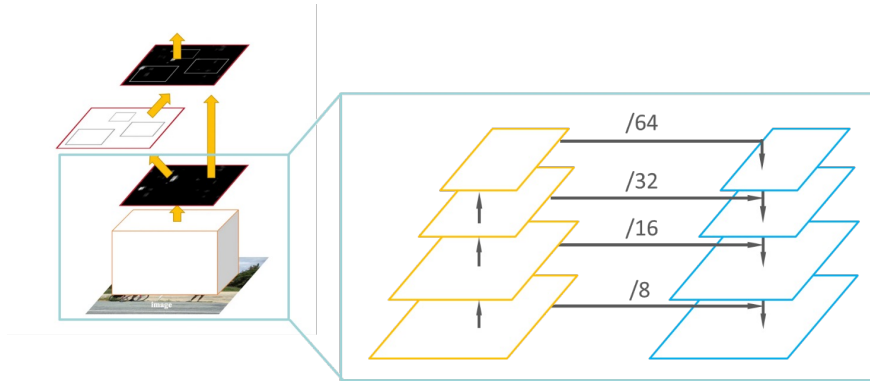


Figure 8: Model architecture

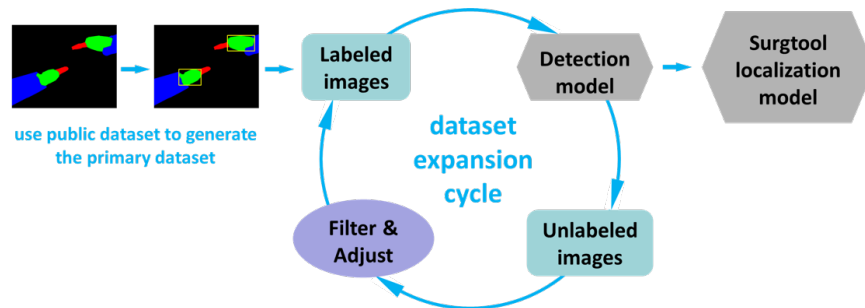


Figure 9: Data expansion scheme

### 3.3 NVIDIA - Team NVIDIA

Team Members: Bo Liu, David Austin, Yiheng Wang, Michal Futrega, Jean-Francois Puget

This team consists of five NVIDIA employees. Three of them (Jean-Francois, David, and Bo) are members of the Kaggle Grandmasters team, with extensive experience in computer vision machine learning competitions. One member (Yiheng) works on MONAI, an open-source framework for deep learning in healthcare imaging. Another (Michal) works on building GPU-optimized models for NVIDIA’s Deep Learning Examples repository<sup>6</sup>. This team’s motivation was to win prizes in both categories using the NVIDIA software stack.

#### 3.3.1 Method Description

Category 1 is a weakly supervised category in the sense that classification labels are given on video level instead of frame level, but test predictions need to be performed on frame level. Since many video-level tools don’t appear in all the frames of the video, the major challenge of Category 1 is to identify frames that contain clean labels. They came up with a unique way to tackle this: first use segmentation models to identify frames where they could identify three unique tools per frame. By identifying three tools, they could then apply the video-level labels to the given frame. In order to do this they used models [26] published from the MICCAI 2017 Robotic Instrument Segmentation Challenge<sup>7</sup>. After applying segmentation models they then used traditional computer vision techniques to count the contours of each unique instrument, and layered additional logic (i.e., instrument contour needs to touch the frame edge) to filter out false positives. All frames where they could positively identify three unique instruments per frame then formed the basis of the training dataset.

<sup>6</sup><https://github.com/NVIDIA/DeepLearningExamples>

<sup>7</sup><https://github.com/ternaus/robot-surgery-segmentation>

Another unique thing in this dataset is the fact that many videos are sequential, e.g., 30-second chunks of a continuous video that last for several minutes or even dozens of minutes. Grouping videos from the same “scene” into the same fold split is critical for meaningful local validation. In order to do this, they compared the image hash of each video’s first frame and the last frame of the preceding video. If the similarity is lower than a threshold, they mark them as from the same scene and put all videos of the same scene into the same split when they split the data into 5 folds. This way, leakage between folds can be prevented. To simulate the test data, they downsampled training videos from fps=60 to fps=1. They also cropped the black empty space on the left and right sides of all the training videos. Then, they blurred out the bottom banner which may contain ground truth labels. Finally, they resized the frames into 640 W x 512 H, the same as the test videos.

After the above steps, the team trained ConvNext[27] Tiny and EfficientNet[28] B4 models, two model architectures that consistently dominate Kaggle image competitions. Standard techniques were used such as cosine learning rate schedule, mixed precision training, mixup augmentations, and weighted loss functions.

Category 2 required localization and classification of a given set of surgical instruments in each frame of a video. Only video-level labels were provided so the challenge can be tasked as a weakly supervised problem. In order to solve this problem they used a diversity of techniques taken from both supervised and unsupervised methods.

One of the key learnings from Category 1 was the importance of sampling rare classes and identifying high-confidence labels in the train set. They exploited these learnings by developing a sample methodology to get a balanced set of frames/labels from a diverse set of scenes using the models they developed for Category 1. After these frames were identified they attempted to get clean localization of the tools of interest through two methods, GradCam[29] and explicit labeling of the tools of interest. GradCam was effective at identifying the clevis of the tools of interest, however, because there was a set of rules and detection logic that needed to be applied on top of the clevis identification (i.e., tip vs clevis detection for some tools and not others), they found that applying manual labels that incorporated these rules were important. GradCam was thus used for visualization only, and manual application of labels and competition logic was used for the start of training.

After identifying clean labels, the team trained YoloV5[30] models first on a small set of manually created labels, according to the example labels on the challenge data page<sup>8</sup>, and then on weakly supervised pseudo-labels predicted from the first set of base models [31]. The workflow is illustrated in Figure 10.

### 3.3.2 Model Training

For Category 1, they trained 5 EfficientNet-B4 models (on 5 fold splits) and 5 ConvNext-tiny models and ensembled them using a trick called logit shift. The idea of the logit shift trick is that, when data is extremely imbalanced between classes as in this dataset, the minor classes’ probabilities are extremely biased towards 0. The extent of the bias can be different across models, making ensembling difficult. Logit shifting is to shift the logit of each class by an optimal constant value (i.e. the same value for the same class, across all samples), so that 0.5 probability threshold is the optimal threshold for the F1 score. This optimal logit shift is tuned on local validation, and is different for each model. When ensembling, they shift logit first on individual models then simply take the average probabilities, since they are already adjusted to be centered around 0.5.

For Category 2, the team trained several versions of YoloV5 and found YoloV5m to be the best performing. Except for the default augmentations such as mixup, mosaic, and HSV transforms, they applied more augmentations like hue saturation value and random brightness contrast to make the model generalize better, especially for the minor tools.

All the experiments for the challenge were trained on NVIDIA DGX Station A100 (with A100 GPUs) and NVIDIA DGX Station (with V100 GPUs).

### 3.3.3 Preliminary Performance

For Category 1, The per-class F1 validation scores of both the ConvNext and EfficientNet models are provided in Table 5, as well as the ensemble score. The final ensemble has a validation score of 0.8526 and

---

<sup>8</sup><https://surgtoolloc.grand-challenge.org/data/>

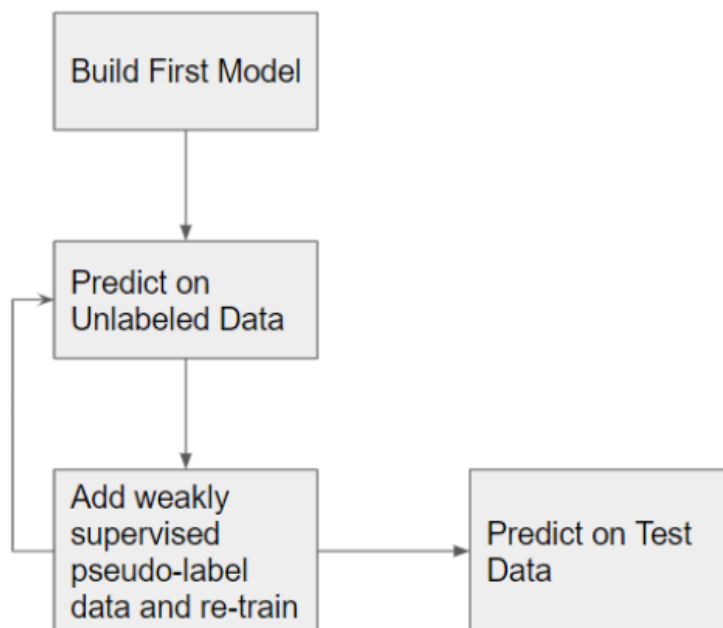


Figure 10: Team NVIDIA Category 2 workflow

a leaderboard score of 0.7055.

For Category 2, the team achieved a mAP validation score of 0.3614 for the first model, and 0.4132 for the retrained model, which translated to a leaderboard score of 0.3058. The validation scores for each class are shown in Table 6.

### 3.4 Argonne National Laboratory - Team ANL-Surg

ANL-Surg team included Neil Getty, Fangfang Xia, Zixuan Zhao, Xiaotian Duan. This team was primarily interested in category 2, though given the available challenges, both categories were considered. ANL-Surg was motivated by the scale of the data, and the interesting need for a weakly-supervised approach. Their initial plan was to use traditional computer vision or pre-trained deep learning models to segment seen tools, and then make label assumptions about the unseen tools and retrain the model iteratively.

#### 3.4.1 Method Description

Training data was sampled at 0.25 FPS and cropped to 880x520 to remove black borders and UI. ANL-Surg used segmentation labels from the two public competitions: MICCAI18: Robotic Scene Segmentation Sub-Challenge [32] and MICCAI17: Robotic Instrument Segmentation [33] for training initial Detectron2 segmentation models.

Their approach for tool presence classification was an ensemble of six ResNet50 models trained using the Fastai framework [34]. Five of the models were trained using cross-validation, and one was trained on all of the data. ANL-Surg averaged the softmax output and used a threshold to determine the final classification.

For tool localization, they trained a Detectron2 [35] model to segment parts of surgical tools. Then the parts were clustered to form bounding boxes for entire tools. Finally, individual tools are cropped out based on the predicted bounding box and query the Category 1 model about the class of the tool (Figure 11).

Table 5: Team NVIDIA Category 1 Results

Class	ConvNext Tiny	EfficientNet B4	Ensemble
needle driver	0.9439	0.9565	0.9487
cadiere forceps	0.6529	0.6826	0.6907
bipolar forceps	0.9236	0.9305	0.9264
monopolar curved scissors	0.9179	0.9330	0.9189
grasping retractor	0.7082	0.6801	0.7188
prograsp forceps	0.7549	0.7946	0.7742
force bipolar	0.9216	0.8665	0.9401
vessel sealer	0.9690	0.9728	0.9805
permanent cautery hook/spatula	0.8602	0.8417	0.8489
clip applier	0.8664	0.8700	0.8439
tip-up fenestrated grasper	0.5333	0.5502	0.5222
stapler	0.9746	0.9748	0.9789
bipolar dissector	0.9787	0.9744	0.9829
suction irrigator	0.8619	0.8306	0.8619
<b>Average F1</b>	<b>0.8476</b>	<b>0.8470</b>	<b>0.8526</b>

Table 6: Team NVIDIA Category 2 Results

Class	Frist model	Weakly supervised model
needle driver	0.5043	0.4933
cadiere forceps	0.5024	0.5111
bipolar forceps	0.3275	0.4441
monopolar curved scissors	0.3568	0.3898
grasping retractor	0.3101	0.4098
prograsp forceps	0.3619	0.4177
force bipolar	0.4341	0.4442
vessel sealer	0.4660	0.4874
permanent cautery hook	0.3866	0.4164
clip applier	0.2536	0.3520
tip-up fenestrated grasper	0.4815	0.4472
stapler	0.2262	0.2902
bipolar dissector	0.1046	0.3197
suction irrigator	0.3448	0.3617
<b>Average mAP</b>	<b>0.3614</b>	<b>0.4132</b>

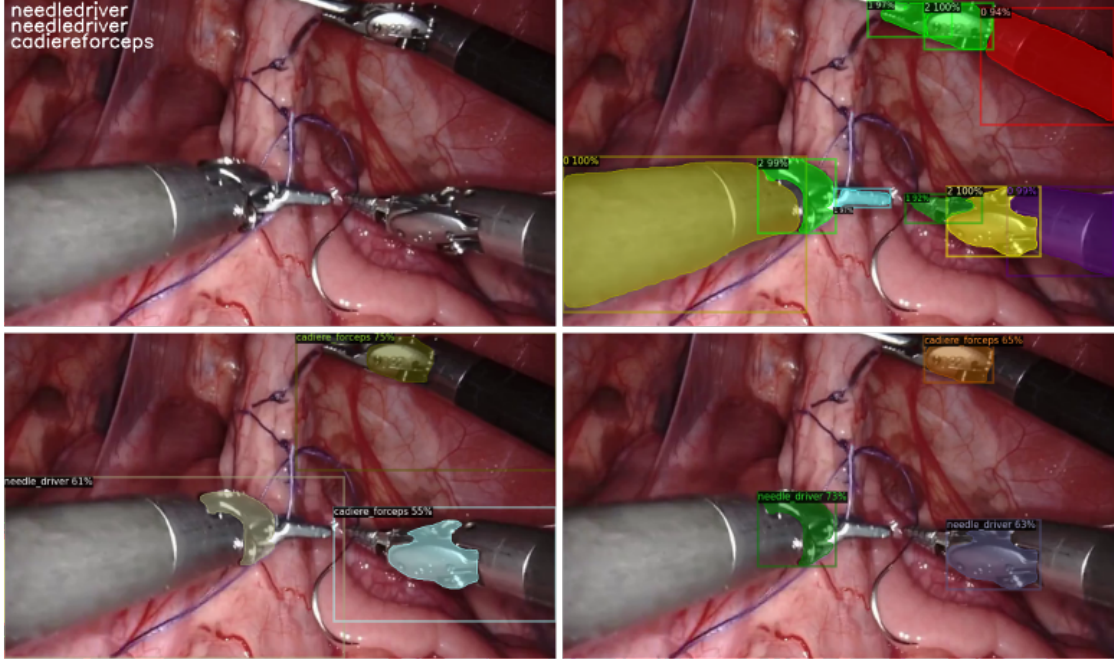


Figure 11: Top right frame is the result of the parts detection model. Bottom left is the instrument tool detection model. Bottom right is the wrist final prediction with post-processing using the Category 1 model.

### 3.4.2 Model Training

ANL-Surg used 5-fold cross-validation, splitting the clips based on their computed similarity scores so that clips of the same video, or very close temporally were not included in both training and validation. However, validation was still a challenge, as a good result may actually be a bad result, due to the many frames with less than 3 visible instruments.

Detectron2 models were trained on a Tesla v100s with 32gGB VRAM for 2000 iterations, a batch size of 20, learning rate of 0.02, and 4 detections per image. MaskRCNN weights were used before finetuning on MICCAI 2017 and 2018 data.

### 3.4.3 Preliminary Performance

Internal validation results for tool presence classification are presented in 7.

Table 7: Preliminary F1 Scores for 5-fold cross-validation for tool presence classification.

Fold	F1
0	0.87399
1	0.91667
2	0.87041
3	0.84748
4	0.86528

## 3.5 Keio University - Team HVRL

Team Members: Ryo Fujii, Ryo Hachiuma, Mana Masuda, and Hideo Saito

The main motivation of the HVRL team was to familiarize themselves with weakly supervised learning in a real surgery environment. The team has experience in building large-scale tool presence detection dataset

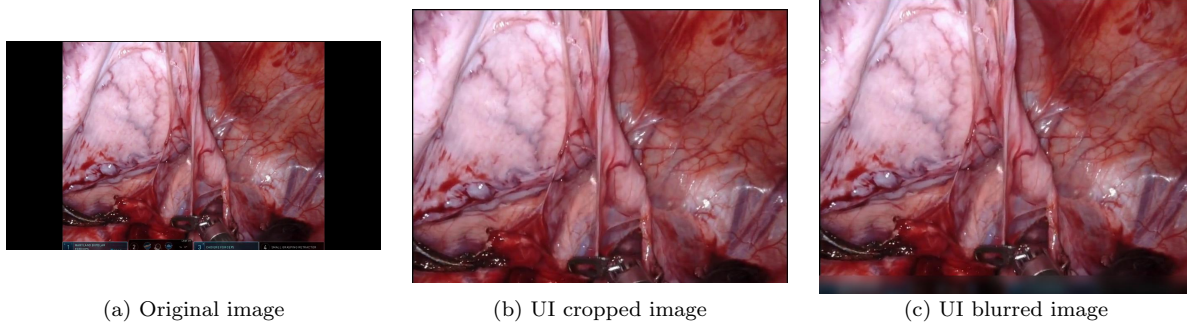


Figure 12: Examples of preprocessing. The original image included the black region on the left and right sides and the tool annotation UI on the bottom. First, the original image was cropped to remove the black region. Then, UI cropping and UI blurring with a probability of 0.5 was randomly conducted.

in open surgery and deeply understand how expensive and tedious to annotate the surgery video [36]. Thus, applying weakly supervised learning reduces the annotation time to a real surgery video.

### 3.5.1 Method Description

For Category 1, multi-label tool presence classification models were trained in a fully supervised manner. Since only video clip-wise annotation is provided, all frames in a video clip were assumed to have the same annotation as the annotation attached to the video clip. The proposed solution was the ensemble of three different models, Swin Transformer V2 [37], EfficientNetV2 [38], and ResNeXt [39], which showed the high performance to the validation data. Models were implemented based on the PyTorch Image Models<sup>9</sup> [40].

For Category 2, Grad-CAM++ [41] was employed for the weakly-supervised tool localization task.

- architecture design: For category1, the team adopted the ensemble of three different models, Swin Transformer V2 [37], EfficientNetV2 [38], and ResNeXt [39]. For Category 2, only EfficientNetV2 was employed.
- data processing, reformatting, transformation, etc.: The image extracted from video clips includes a black region on the left and right sides and a tool annotation UI on the bottom. Firstly, these black regions were removed. Then, UI cropping and/or UI blurring with a probability of 0.5 were randomly conducted. These procedures prevented the model from getting the tool presence information from the UI directory. Examples are shown in Fig. 12.
- data augmentation: several data augmentation techniques were applied for achieving robust training. Specifically, the team applied the data augmentation techniques shown in Table 8. These augmentations were applied to train all models.
- model inputs: RGB image.
- model outputs: For category 1, multilabel output. For category 2, pixel-wise heatmap.
- model loss function: For category 1, binary cross-entropy loss. For Category 2, the model trained by Category 1 was used.
- model pre-training: For category 1, The weights of Swin Transformer V2 and EfficientNetV2 were initialized with the weights trained with ImageNet [42], and that of ResNeXt was initialized with the weights trained with Instagram Datasets. For Category 2, the model trained in Category 1 was reused.
- post-processing: For category 1, test time augmentation (TTA) was employed (Table 8). For category 2, the gradient for the last convolutional layer and the penultimate convolutional layer was computed

<sup>9</sup><https://github.com/rwightman/pytorch-image-models>



via back-propagation. After obtaining the pixel-wise heatmap for each layer, these two heatmaps are averaged to obtain the final heatmap. Then, the heatmap is binarized with threshold  $\sigma = 0.5$  to obtain the binary map. Finally, the connected component algorithm is applied in order to extract multiple bounding boxes from the binarized heatmap.

- Hyper-parameters (Table 9): For Category 1, Stochastic Gradient Descent was employed as the optimizer, with the momentum 0.9, weight decay 0.0001, and cosine annealing strategy. For the learning rate, batch size, and training epochs, different settings on three methods were used as shown in Table 8. For Category 2, the model trained in Category 1 was used, thus retraining was not conducted.

Table 8: Data augmentation

Augmentation	Range	Probability
Horizontal flip		0.5
Color shift	30	0.5
HSV Shift	20	0.5
Brightness	[0.1, 0.3]	0.2

Table 9: Hyperparameters

methods	learning rate	batch size	epochs
Swin Transformer V2	0.6	24	50
EfficientNetV2	0.57	48	30
ResNeXt	0.36	192	50

The trained model outputs a multi-class label. The Grad-CAM++ [41] module generated the class activation maps. Then, the generated class activation maps with threshold  $\sigma = 0.5$  generated the binary map. Finally, a connected component algorithm was applied in order to extract multiple bounding boxes from the binarized heatmap.

### 3.5.2 Preliminary Performance

Table 10: Local validation results with different models.

Method	F1-score
Swin Transformer V2	0.925
EfficientNetV2	<b>0.930</b>
ResNeXt	0.928
Model ensemble	<b>0.930</b>

Table 10 summarizes the results against the local validation data. Models which showed the best performance on the local validation data were chosen. Specifically on epochs 17, 25, and 23. The table shows that a single EfficientNetV2 and the ensemble of three models achieved the highest F1-score.

## 3.6 Muroran Institute of Technology - Team SK

Team Members: Satoshi Kondo, Satoshi Kasai, and Kousuke Hirasawa

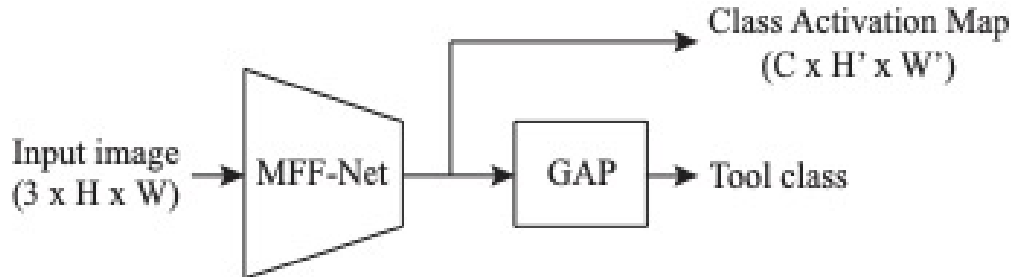


Figure 13: Overview of our proposed method.

### 3.6.1 Method Description

Team SK proposed a weakly-supervised surgical tool localization method with a multiplicative feature fusion network. The network was trained to learn the presence of surgical tools in the input image with supervised learning. When detecting surgical tools (task in Category 1), this method predicts the presence of surgical tools by using the trained network. When localizing surgical tools (task in Category 2), this implementation first predicts the presence of surgical tools and then checks the class activation map corresponding to the predicted surgical tool, localizing the tool by thresholding the activation map, i.e., in a weakly-supervised manner.

Figure 13 shows the entire structure of the proposed network. Multiplicative Feature Fusion Networks (MFF-Net) [43] was used as the base network. MFF-Net is designed to aggregate features at different levels, which generates the class activation map (CAM) and categorical features for classification. Then, a CAM of the size  $C \times H' \times W'$  is obtained. Here,  $C$  is the number of classes in the tool classification, and  $H'$  and  $W'$  are the height and width of the CAM, respectively. ResNet-50 is used as the backbone of the MFF-Net. The training and prediction are performed frame-by-frame base although the input data is video.

The network was then trained by using the provided dataset, which has images and labels showing the presence of tools in the images. There were 14 surgical tools and 3 tools are shown in an image at most. Based on the team’s observation that two “needle driver” tools are often shown in the same images, the model was trained not as a 14-class classification model but as a 15-class classification model, i.e.,  $C = 15$ . Since the dataset contains two “needle driver” classes in 15 classes. When only one needle driver is shown in the input image, only the first label in needle driver classes is active, i.e., give 1 as the ground truth label. When two needle drivers are shown in the input image, both labels for needle driver classes are considered active.

In inference, the probabilities of surgical tool presence were obtained from the CAMs through global averaging pooling and sigmoid activation. Tool classes whose probabilities are higher than the threshold (0.5) were selected. In this case, the selected tool classes were the results of the surgical tool detection task (Category 1). For the selected tools, this approach obtained CAM of the corresponding tool class in the order of the probability (from the highest probability to the lower ones). Then, the tool area was obtained by thresholding the CAM. The threshold was determined by using Otsu’s binarization method. After identifying the bounding box surrounding the tool area, the IoU was calculated. If the IoU value is less than the threshold, the bounding box is employed as the result of the surgical tool localization (Category 2).

### 3.6.2 Model Training

For the training of the network, the team constructed a dataset by sub-sampling images from videos. The total number of images for training in this set was over 150k, being split into training and validation in an 8:2 ratio.

The augmentations techniques used were horizontal flip, shift, scale, rotation, color jitter, Gaussian blur, and Gaussian noise. The augmented images were resized to  $640 \times 480$  pixels. The employed optimization method was Adam, and the initial learning rate was set to  $1.0 \times 10^{-5}$  changing at every epoch with cosine annealing. The cross-entropy loss was used as the loss function. The batch size was set to 64 and the number of epochs to 30. The model taking the lowest loss value for the validation dataset was selected as the final

model. Five models were trained by using 5-fold cross-validation, and CAMs obtained by five models were averaged in inference. An NVIDIA RTX3090 GPU for the training.

### 3.6.3 Preliminary Performance

When using the evaluation system provided by the challenge organizers, the F1 score was 0.816 for Category 1 (surgical tool detection). For Category 2 (surgical tool localization), mAP was 0.03.

## 3.7 Team VANDY-VISE

Team Members: Xing Yao, Ange Lou, Hao Yang, Jintong Han, Jack Noble, Jie Ying Wu

The goal was to take full advantage of the auto-correlation and cross-correlation between various frame-to-frame and video-to-video to solve this weakly supervised recognition problem. Therefore, an attention-based learning framework was selected to capture and detect causal features that were directly related to surgical tool detection. No public dataset apart from the challenge dataset was used in this work.

### 3.7.1 Method Description

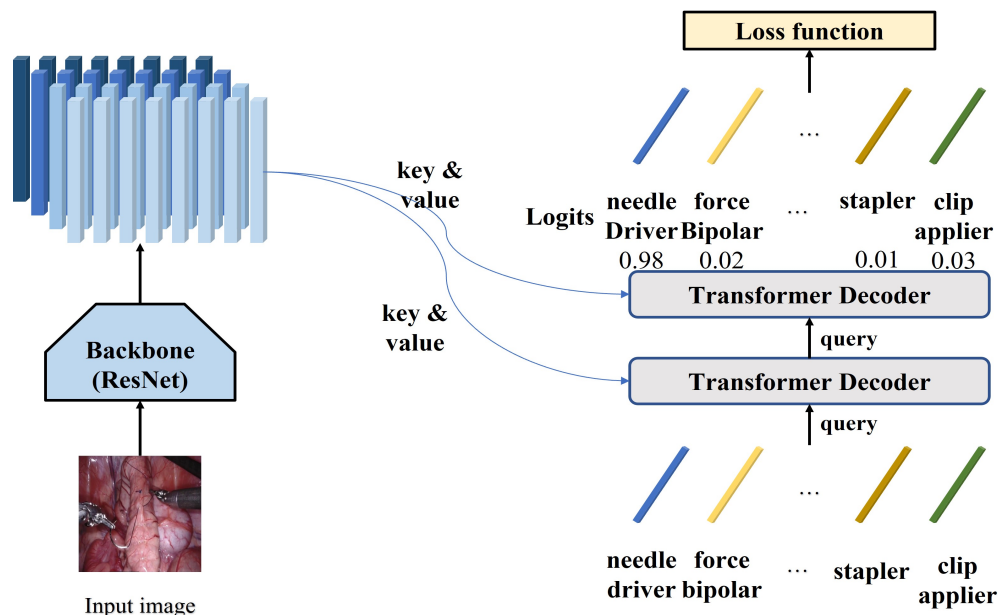


Figure 14: Architecture of Query2Label [44]

The VANDY-VISE team leveraged the same framework as Query2Label[44] to do multi-label classification and localization (shown in Figure 14). The input image  $x$  was first sent through a ResNet backbone [45] to extract the spatial features. The extracted spatial features were then sent into the transformer along with each of the label embeddings. The transformer decoders generated attention maps by comparing label embeddings with spatial features, then pooling the spatial features by linearly combining these spatial features based on the attention map. After obtaining spatial features of the input image, each label embedding was sent to the transformer decoder to query and pool the desired feature. Finally, those features went through a linear projection layer to compute the logits for each class.

For a given image  $x \in R^{H \times W \times 3}$ , a ResNet backbone was used to extract spatial features  $f_0 \in R^{H_0 \times W_0 \times d_0}$  from the input image. Here,  $H \times W$  and  $H_0 \times W_0$  represented the height and width of the input image and extracted features respectively, while  $d_0$  denoted the dimension of features. The spatial features were then projected from  $HW \times d_0$  to  $HW \times d$  by using a linear projection layer, where  $d$  was the desired feature dimension.

The class embedding was applied as a query that had dimension  $Q^{K \times d}$ . Here  $K$  represented the number of classes. Then the cross-attention was calculated between the spatial features and queries to pool the class-related features by using multi-layer transformer decoders. In the implementation carried out by the Vanderbilt University team, the standard transformer decoder comprised cross-attention, self-attention, and a position-wise feedforward network. The transformer decoder,  $i$ , updated the queries  $Q_{i-1}$  as following:

$$\begin{aligned} \text{self-atten} : Q_i^{(1)} &= \text{MultiHead}(\tilde{Q}_{i-1}, \tilde{Q}_{i-1}, Q_{i-1}) \\ \text{cross-atten} : Q_i^{(2)} &= \text{MultiHead}(\tilde{Q}_{i-1}^{(1)}, \tilde{f}, f) \\ \text{FFN} : Q_i &= \text{FFN}(Q_i^{(2)}) \end{aligned}$$

where the hat represented variables with position encoding.

The query feature  $Q_i$  was sent to a linear projection layer to a logit value for each class.

$$p_k = \text{Sigmoid}(W_k^T Q_{i,k} + b_k)$$

in the right-hand-side of the function,  $W_k$  and  $b_k$  were parameters of the linear projection layer. The left-hand side,  $p_k$ , was the predicted probability of each class.

In the implementation, a simplified asymmetric loss [46] was applied as shown below:

$$L = \frac{1}{K} \sum_{k=1}^K \left\{ \begin{array}{l} (1 - p_k)^{\gamma+} \log(p_k), y_k = 1 \\ (p_k)^{\gamma-} \log(1 - p_k), y_k = 0 \end{array} \right\}$$

here,  $y_k$  was a binary label for  $k$  classes, which corresponds to the  $\gamma$  value to choose. By default, they are set to  $\gamma+ = 0$ ,  $\gamma- = 1$ . It was noteworthy that countless noisy labels existed in the training annotations, and it was very time-consuming to remove them manually. Most of the label noise came from pseudo-labels that were not present in the videos. Based on this prior knowledge, during the training phase of the classification model, for videos with more than two labels, the team removed the largest loss among all existing labels. Compared with the original loss, this method improved the best validation mAP from 0.953 to 0.966.

In this work, the VANDY-VISE team post-processed the cross-attention weights created by the transformer decoder to generate bounding boxes for each predicted class. The post-processing included sparse matrix processing and bounding box generation based on OpenCV [47]. During the attention visualization process, the cross-attention weights matrix  $M$ , produced by the decoder, was initially reshaped from dimensions  $B \times C \times HW$  to  $B \times C \times H \times W$ . This transformation enabled the representation of cross-attention between each pixel and its respective class. Then, according to the classification results of the model, the classes in the normalized attention map were filtered, and only the classes with predicted True were retained. Because tools of different categories shared similar morphological features, the attention maps of different categories still had similarities. To further distinguish the critical vector of each class, for different positions of the same class, this method selectively retained one or several positions with the highest energy; for the exact position of different classes, it only retained the position corresponding to the class with the highest energy. Finally, the team binarized the sparse attention maps and used `cv2.findContours` and `cv2.boundingRect` [47] functions to generate corresponding bounding boxes.

### 3.7.2 Model Training

To make the problem more tractable, one frame from each video clip was randomly selected to build a relatively smaller dataset, which in total contained 24695 images. From this whole set, 3000 images were randomly partitioned as the validation set, and the rest 21695 frames were assigned to the training set. Blank areas in each frame were removed. Furthermore, AdamW was chosen as the optimizer with a learning rate of 1e-4. The training batch size was 32. All experiments were based on Pytorch and trained with a single RTX A5000 GPU.

### 3.7.3 Preliminary Performance

In multi-label classification tasks, the loss decreased steadily during the training phase, and the Vanderbilt University team achieved 0.966 mAP and 0.955 F1 scores on their validation set and a 0.6202 F1 score on the given test set. For the localization task, their algorithm (multi-head attention weights map) could localize all surgical tools that appear in the given validation video.

## 3.8 University Medical Center Hambrug-Eppendorf - Team UKE

Team Members: Maximilian Nielsen, Samuel Schüttler, Thilo Sentker, Hümeyra Husseini, Ivo Baltruschat, Rüdiger Schmitz, René Werner

### 3.8.1 Method Description

Recently, self-supervised deep learning gained attention by setting new benchmarks for different image classification tasks, showing potential for further investigation in related domains [48, 49]. Different to supervised methods, self-supervision does not directly produce a meaningful output (e.g., a classification result or segmentation mask), but solely a representation, i.e. a feature-vector, of the input. To find an expressive representation of the input, such methods predominately rely on contrastive learning, which is characterized by forcing the model to output similar representations for different augmented versions of the same input. Advantages compared to supervised learning approaches are a relative strong performance with a fraction of labeled data and a high degree of generalizability. Therefore, a self-supervised approach for both tasks of the SurgToolLoc challenge was employed. More specifically, deep image representations are extracted by self-supervised vision transformers (DINO). Subsequently, downstream classification is performed by a machine-learning classifier that is fitted on the model output of a smaller subset of labeled data. For tool localization, the individual outputs of the trained attention heads to generate bounding boxes were exploited.

For both tasks, the starting point was to extract feature vectors exploiting a self-supervised learning approach based on DINO (cf. figure 15 for a schematic illustration). Prior to training, frames were resized to  $308 \times 208$  px and frame intensities normalized to  $(-1, 1)$ . A DINO model, pre-trained on the ImageNet data, was trained on the given pre-processed training data with slightly adapted default DINO-parameters.

Several image augmentation techniques were utilized to improve the robustness of the model. The DINO augmentation techniques included random cropping to simulate different perspectives, solarization to introduce variations in brightness, flipping to incorporate left-right reversal, Gaussian blurring to mimic real-world blurs and color jittering to introduce variations in color.

A temporal global crop was applied to consider the temporal components of the input data. This approach involves randomly selecting a global crop from a frame that is in temporal correspondence with the input frame, with a tolerance of  $\pm 5$  s. This approach ensures temporal consistency between the input frame and the selected global crop, i.e. the temporal structure of the data is preserved which further diversifies the input data.

The loss function used was the DINO loss, which is a combination of temperature-weighted cross-entropy and feature normalization. The temperature-weighted cross-entropy term ensures a sharp feature distribution in the latent space, while the feature normalization term stabilized the training process and improved generalization by enforcing uniformity.

For task 1, a machine-learning classifier (logistic regression) was fitted on the DINO model output of a smaller subset of labeled data to learn the relationship between extracted feature vectors and corresponding training labels. Hyper-parameter optimization, feature selection and decision threshold optimization using a differential evolution algorithm were performed.

For task 2, a linear combination between multi-head attentions, RGB-values and minimum RGB-value to gray-value-distances was optimized to match the EndoVis 2017 instrument segmentations (shaft, tip, clevis) [50]. Subsequently, bounding boxes for the three largest connected components were extracted from the resulting segmentations. For each crop, a pseudo-label was created from possible ground-truth values and similar other crops (DINO latent space). The tool classifier was trained as in task 1.

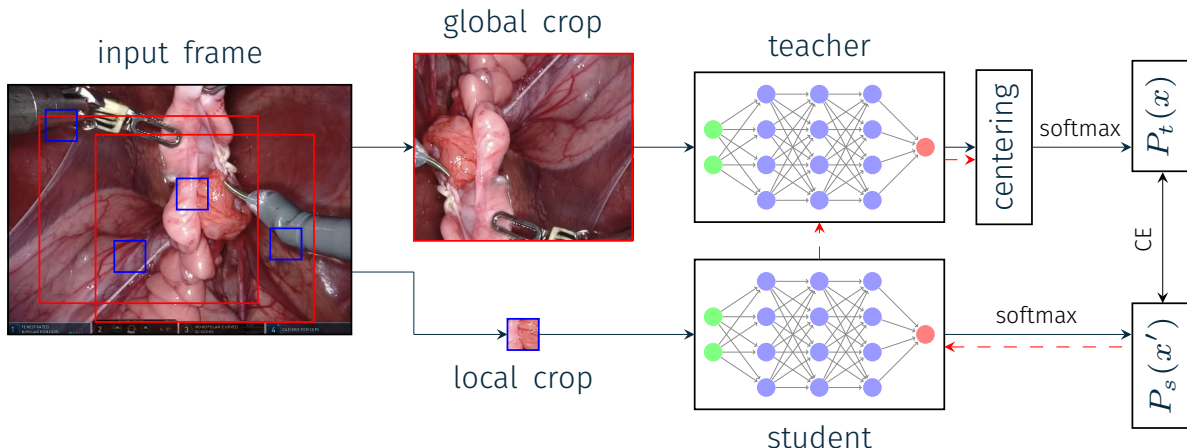


Figure 15: DINO-based self-distillation. Global and local crops are extracted from the input frame, individually augmented and fed into the teacher and student model, respectively. Note that a temporal global crop was used, i.e. the global crop is randomly extracted out of one frame that is in temporal correspondence to the input frame ( $\pm 5$ s) to achieve temporal consistency. Further, the applied softmax function has a temperature parameter to control the sharpness of the output probabilities. After training, a machine-learning classifier is fitted on the DINO model output of a smaller subset of labeled data. For more details cf. the corresponding DINO-publication [48].

### 3.8.2 Model Training

The model was trained for a total of 30,000 epochs using a batch size of 224 on a GPU server equipped with an A40 GPU, 1TB of RAM, and a CPU with 64 cores. Model training took about 35 hours.

To ensure a deterministic output and a fair comparison between different runs, a fixed random seed, i.e. sum of int32 interpreted sha256-hash of string “STL-Challenge”, was used throughout model training. Thus, consistent results for each run were obtained and it was possible to compare the performance of different models in a controlled environment.

### 3.8.3 Preliminary Performance

Applying the proposed algorithm on the self-assessed validation split containing 30% of the provided video data yielded a F1-score for task 1 of **0.82**. For task 2, validation was not possible as ground truth values were not available.

## 3.9 Furtwangen University - Team ITeM

Team Members: Tamer Abdulbaki Alshirbaji, Nour Aldeen Jalal, Herag Arabian, Ning Ding, and Knut Moeller

The ITeM team is composed of four PhD students who are currently working under the guidance of Prof. Knut Moeller at the Institute of Technical Medicine, Furtwangen University, Germany. ITeM team members are involved with research projects in collaboration with industrial and clinical partners. These projects aim to develop and integrate smart technologies into the current setup inside the operating rooms (OR). Analyzing surgical videos using deep learning approaches, particularly surgical workflow recognition, represents a core topic that has been addressed by the researchers at ITeM. Spatio-temporal deep learning approaches for surgical tool classification and phase recognition have been developed. Additionally, data fusion approaches have also been investigated on data from surgery and anesthesiology. Therefore, participation in the **SurgToolLoc** challenge represents a great opportunity for the ITeM team to evaluate developed

approaches on a new challenging dataset and to be in contact with other highly qualified teams from around the world.

### 3.9.1 Method Description

The SurgToolLoc challenge addresses supervised tool classification and weakly-supervised tool localization tasks in laparoscopic videos. In both tasks, only binary labels for tool presence can be used to train the proposed model. Similar to other public datasets (e.g., Cholec80 [51]), surgical tool presence is imbalanced, which will cause a bias on the trained model to high-representative tools. Additionally, tool classification is a multi-object classification task, where up to 4 tools may appear in the laparoscopic image. Moreover, the model will be tested with images from video clips that are not included in the training data.

A deep learning pipeline that addresses all the above-mentioned challenges was developed. The model consisted of the ResNet-50 architecture as a backbone model since it showed better performance over other CNN architecture for the tool classification task [52]. For weakly-supervised tool localization, the algorithm was built upon the work of Durand et al. [53] and the follow-up approaches by Vardazarya et al. [54] and Nwoye et al. [55], but introduced novel modifications. First, attention modules were adopted to the base CNN model to help generate better-refined features. Second, features from multiple stages (i.e., from lower and top layers) were fused for a better representation of laparoscopic images' contents. Third, a novel spatial pooling was applied to obtain tool presence confidence from the localization maps. Finally, a new loss function was proposed to model possible tool combinations of each video frame (Figure 16 shows the architecture of the proposed model).

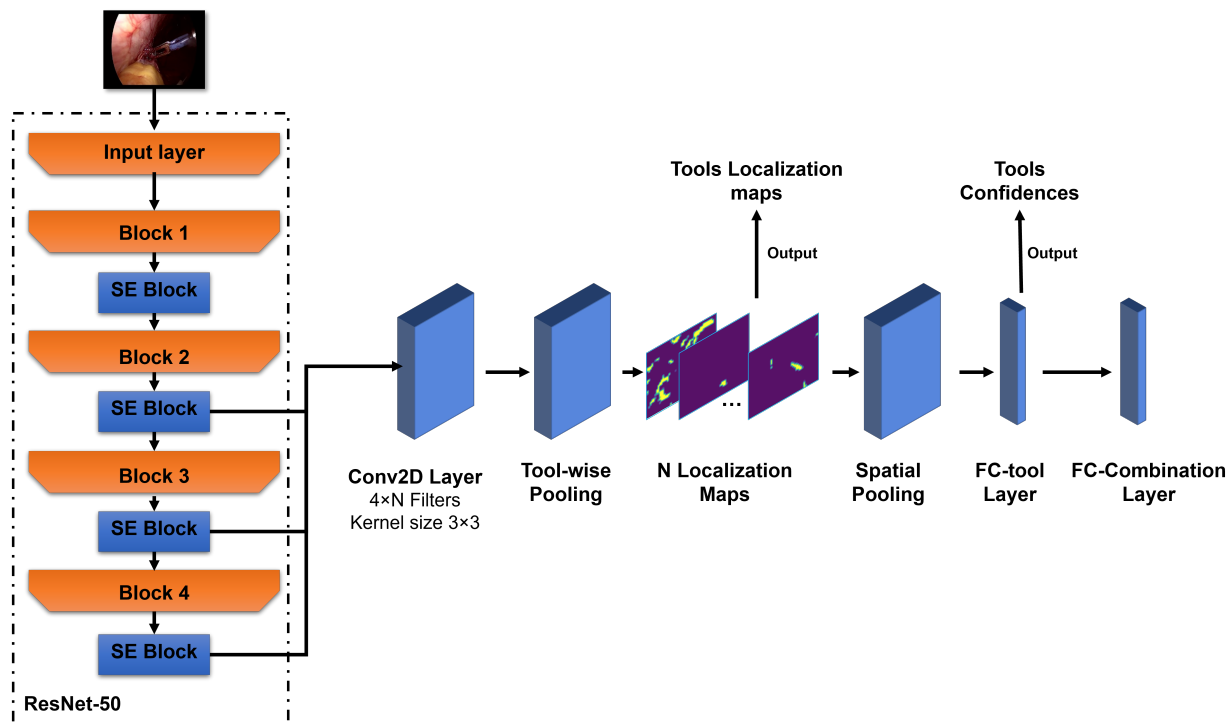


Figure 16: The complete pipeline of the proposed model for tool presence detection and localization. SE blocks represent the squeeze-and-excitation attention modules; the Conv2D layer is the multi-map localization layer; FC-tool and FC-Combination layers are the fully-connected layers employed to obtain confidence values of the tool presence and tool-combination, respectively. N is the number of tool classes defined in the dataset (N=14).

- architecture design

- base model

The proposed architecture was built on the base CNN model ResNet50 [56]. This model showed competitive performance for surgical tool classification in laparoscopic images [52]. ResNet50 consists of five convolutional blocks and on top a global average pooling and a fully-connected layer. The shortcut connections used in the model lead to more efficient optimization and higher accuracy [56]. The model input was increased to  $375 \times 300$  instead of  $224 \times 224$ . Additionally, the stride of convolutional layers was set to 1x1 in the last two blocks. Due to these modifications, higher spatial resolution is preserved at deeper layers.

- squeeze-and-excitation module

Squeeze-and-Excitation (SE) [57] attention modules were integrated into the convolutional architecture to boost the model performance. Four SE modules were added after the fourth, seventh, thirteenth, and sixteenth convolutional blocks. The reduction ratio was set to 16 in all SE modules.

- multi-stage feature fusion

In conventional methods, the CNN model performs the classification based on information learned at the last layer. In fact, features of deeper layers encode semantic information about classes. On the other hand, features of shallow and intermediate layers encode some generic information. Feeding such information for instance to a classification layer can support the classification decision [58]. Thus, in this approach, features at the output of the second, third, and fourth attention modules were combined forming a feature bundle. The combined features were passed to a batch-normalization layer.

- Conv2D layer

A convolutional layer was used to transfer the multi-stage features to a localization map for each class. The convolutional layers had a kernel size of 3x3. The number of filters was set to  $M \times N$ , where  $M$  is the number of maps for each class and  $N$  is the number of tool classes ( $N=14$ ).  $M$  was set to four, thus, four localization maps were generated for each surgical tool. In these convolutional layers, the stride was set to 1x1 to preserve the spatial resolution.

- pooling operations

To generate one localization map and presence confidence for each tool, tool-wise pooling, and spatial pooling operations were applied consecutively. The max operation was applied across the 4 localization maps of every tool. The input and output of this operation are  $w \times h \times 4N$  and  $w \times h \times N$ , respectively, where  $w$  and  $h$  represent the spatial dimension of the obtained feature maps, while  $N$  is the number of tool classes in the dataset.

Special spatial pooling (equations 3.9.1, 3.9.1) was then applied to transform the map of each tool into two features. These two features represent the positive evidence ration (PER) and the negative evidence ratio (NER), and they were provided into a fully-connected layer with a Sigmoid activation to obtain tool-wise confidence values.

$$\begin{aligned}
 PER &= \frac{\sum_i^h \sum_j^w x_{i,j}}{h.w} & \iff & \begin{aligned} x_{i,j} &= 1 \text{ for } x > 0.9 \\ x_{i,j} &= 0, \text{ Otherwise} \end{aligned} \\
 NER &= \frac{\sum_i^h \sum_j^w x_{i,j}}{h.w} & \iff & \begin{aligned} x_{i,j} &= 1 \text{ for } x < 0.1 \\ x_{i,j} &= 0, \text{ Otherwise} \end{aligned}
 \end{aligned}$$

where  $h$  and  $w$  are the spatital dimension of the localization maps,  $x_{i,j}$  is the pixel value at  $i$  and  $j$  position.

- fully-connected (FC) layers

Two fully-connected (FC) layers were added on top of the spatial pooling layer. The first FC layer (FC-tool) performs the tool presence detection and contains 14 nodes since 14 tools are defined in the dataset. The confidences obtained from the FC-tool were then provided into the second FC layer, termed FC-Combination), which was added to model the possible tool combinations in the dataset. Therefore, tool-combination classes were generated for all images prior to training the model. First, all possible tool combinations were extracted from the provided tool classes with their corresponding distributions. Then, 14 tool combination classes were generated. The



first 13 classes represent the combinations of the highest thirteen distributions and the last class represents the remaining combinations.

- data pre-processing  
The video clips provided had a frame rate of 60 frames per second (FPS). Training images were extracted at 1 fps. Since some clips contained black frames, these frames were identified and excluded. The label provided for every clip was assigned to its corresponding frames.  
The image pre-processing included cropping out the black sides of the images, blurring the user interface (UI) information appearing at the bottom of the images, resizing the image into the model input ( $375 \times 300 \times 3$ ), and image normalization.
- model input: The input of the model is an image of size  $375 \times 300 \times 3$ .
- model outputs: The outputs of the model are confidences of the 13 tool categories defined in the dataset and localization maps of detected tools.
- model loss function: Two loss functions were employed in this study. The binary cross-entropy function was used to compute the loss of each tool class, as in Eq. 3.9.1. To reduce the imbalanced data effect, loss-sensitive learning approach [59] was applied. Here, the loss of each tool was multiplied by a weighting factor that was estimated according to the tool-appearance distribution in the training data. Additionally, the Softmax cross-entropy loss was utilized to calculate the classification error for the tool combination (Eq. 3.9.1).

$$Tool_{loss} = \frac{-1}{B} \sum_{n=1}^B \sum_{t=1}^T w_t [l_t^n \log(C_t^n) + (1 - l_t^n) \log(1 - C_t^n)]$$

where  $Tool_{loss}$  is the total loss of all tools,  $B$  is the batch size,  $T$  is the number of tools in the dataset,  $w_t$  represents the loss-weight calculated for every surgical tool,  $l_t^n = [0, 1]$  is the tool presence ground truth, and  $C_t^n$  is the tool presence confidence obtained from the spatial pooling operation.

$$loss_{comb.} = \frac{-1}{B} \sum_{n=1}^B \sum_{c=1}^C G_c^n \log \sigma(C_c^n)$$

where  $loss_{comb.}$  is the total loss of tool-combination category,  $B$  is the batch size,  $C$  is the number of defined tool-combination in the dataset,  $G_c^n$  is the ground truth of image  $n$ ,  $C_c^n$  is the output of the FC-Combination layer, and  $\sigma$  represents the softmax activation function.

- model pre-training: The base ResNet-50 model was pre-trained with the Cholec80 [51] dataset. The weights of the newly added layers were randomly initialized.
- post-processing: post-processing step was required to extract bounding boxes from the localization maps generated after applying the tool-wise pooling operation. Localization maps of the tools that were detected to be present in the image (confidence  $> 0.5$ ) were extracted. A Gaussian filter with  $\sigma = 1.0$  was applied to smooth boundaries in the localization maps. Then, a binary mask was generated by thresholding the localization map with a threshold of 0.5. Bounding boxes were finally generated on top of generated masks. For the *needle driver* tool, up to two bounding boxes were considered.

### 3.9.2 Model Training

The Adam optimizer with cyclical learning rate techniques was utilized. The cyclical learning rate boundaries were chosen as 0.005 and 0.001, and a step-size of  $4 \times iteration - per - epoch$  was chosen. The model was trained with a batch size of 50 images for 50 epochs. Images were shuffled for every epoch. All implementations and experiments were accomplished in Keras framework with Anaconda virtual environment platform and run on a desktop with an AMD Ryzen Threadripper PRO 3955WX 16-Cores 3.90 GHz, 512 GB RAM, and 64-bit Windows 10 Operating System with an NVIDIA RTX A6000 graphics processing unit (GPU).

### 3.9.3 Preliminary Performance

To evaluate the trained models prior to submission, a small, denoised-label dataset was created by manually revising the provided labels. Figure 17 shows the performance of the proposed model for surgical tool classification on the validation set. Additionally, the results of different models on the preliminary-test data are presented in Table 11.

The experimental results of the proposed model showed high performance on both the validation and preliminary test data. However, an extensive ablation study is still required to show the advantage of every component of the model. Moreover, additional work should be done to denoise the tool labels provided.

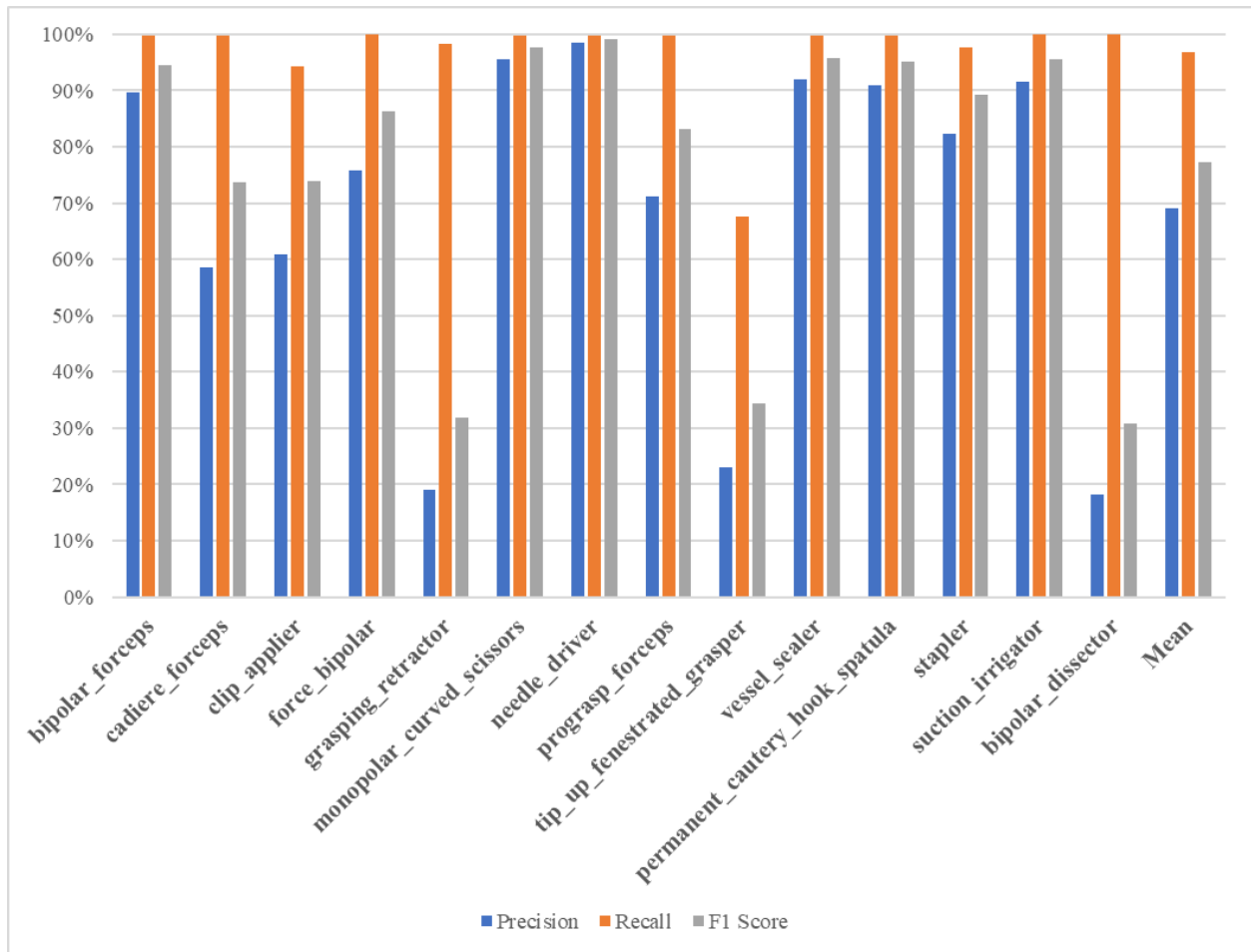


Figure 17: Model performance on the validation data.

Table 11: The results of the different models obtained from the preliminary test

Model	F1-Score (%)
Base model	51.76
Base model+Conv2d+Pooling	76.23
Base model+Conv2d+Pooling+SE	77.51
Final Model	84.35

### 3.10 Shun Hing Institute of Advanced Engineering - Team Medical Mechatronics (MM)

Team Members: An Wang, Mengya Xu, Mobarakol Islam, Long Bai, Winnie Pang, Hongliang Ren.

#### 3.10.1 Method Description

Multi-label tool classification from surgical videos is challenging but demanding to increase the autonomy of computer-assisted interventions. The method from Medical Mechatronics (MM) utilized the hybrid ViT [60] model (R50-ViT-B\_16)<sup>10</sup> to complete the classification task. Further, the team considered solving the noise and imbalance issues of the dataset by intentionally splitting the dataset into training and validation and with an unbalanced dataset sampler during training. They also applied augmentations like Cutout [61], and RandAugment [62], to increase generalization.

There are always dataset issues like noisy labels, imbalanced datasets, and domain shifts in the practical dataset. It is important to consider proper data cleaning and manipulation before feeding the data to the deep learning models. The entire training dataset consists of over 20 thousand videos. There are 14 types of tools in these videos. The frequency of their appearance is quite different, making the dataset imbalanced. The first frame from each valid video (except for 9 corrupted videos) was extracted to represent each video clip to reduce redundancy and save memory. The corresponding label of each frame is a one-dimensional array with a length of 14. The element of the respective class was set to 1 if the tool exists and 0 otherwise. The dataset was not randomly split into training and validation sets. Instead, the team analyzed the dataset and ensured all tools existed in the training and validation periods. The number of training samples was about 80% of the entire dataset, and the number of each class of samples for training was also around 80%.

The training images were resized to 224X224, and two advanced augmentation techniques, i.e., Cutout and RandAugment, were incorporated as data augmentation to avoid overfitting. The PyTorch-based multilabel balanced sampler<sup>11</sup> was adopted to sample the samples during training. Asymmetric Loss (ASL) [63] was used as the multi-label classification loss function, which performs differently on positive and negative samples by automatically reducing the weight and hard limit of easy negative samples, and eliminating samples that could be mislabeled. Figure 18 describes their model architecture.

#### 3.10.2 Model Training

During training, SGD was used as the optimizer, and a cosine scheduler was applied to the learning rate (max learning rate was 3e-2) for 1000 warm-up steps. The total number of training steps was 10000. The hybrid ViT model was trained on one RTX3090 GPU with a batch size of 128, taking around 3.5 hours to finish the training. The balanced multi-label sampler in the dataloader helped achieve training-time class balancing. The evaluation interval was set to 50 steps, and the final model was acquired from the step with the highest validation MAP.

#### 3.10.3 Preliminary Performance

An mAP of 0.86 was achieved on the validation dataset. Figure 19 shows the training process.

### 3.11 Bin Zayed University of Artificial Intelligence - Team BioMedIA

Team Members: Aleksandr Matsun\*, Mugariya Farooq\*, Numan Saaed, Jose Renato Viera Restom and Mohammad Yaqub

The team was focused on the task of tool classification but they targeted the localization task as well considering the extent to which the task of localization could help the classification problem. The authors experimented with simple architectures like ResNet 50 first and planned to build on these simple architectures to increase the performance of the model. In the end, the team used a combination of two architectures: ConvNext and Yolov5 which helped them improve the performance metrics.

<sup>10</sup>[https://github.com/mobarakol/Hybrid\\_ViT](https://github.com/mobarakol/Hybrid_ViT)

<sup>11</sup><https://github.com/issamemari/pytorch-multilabel-balanced-sampler>

## R50+ViT-B/16 hybrid model

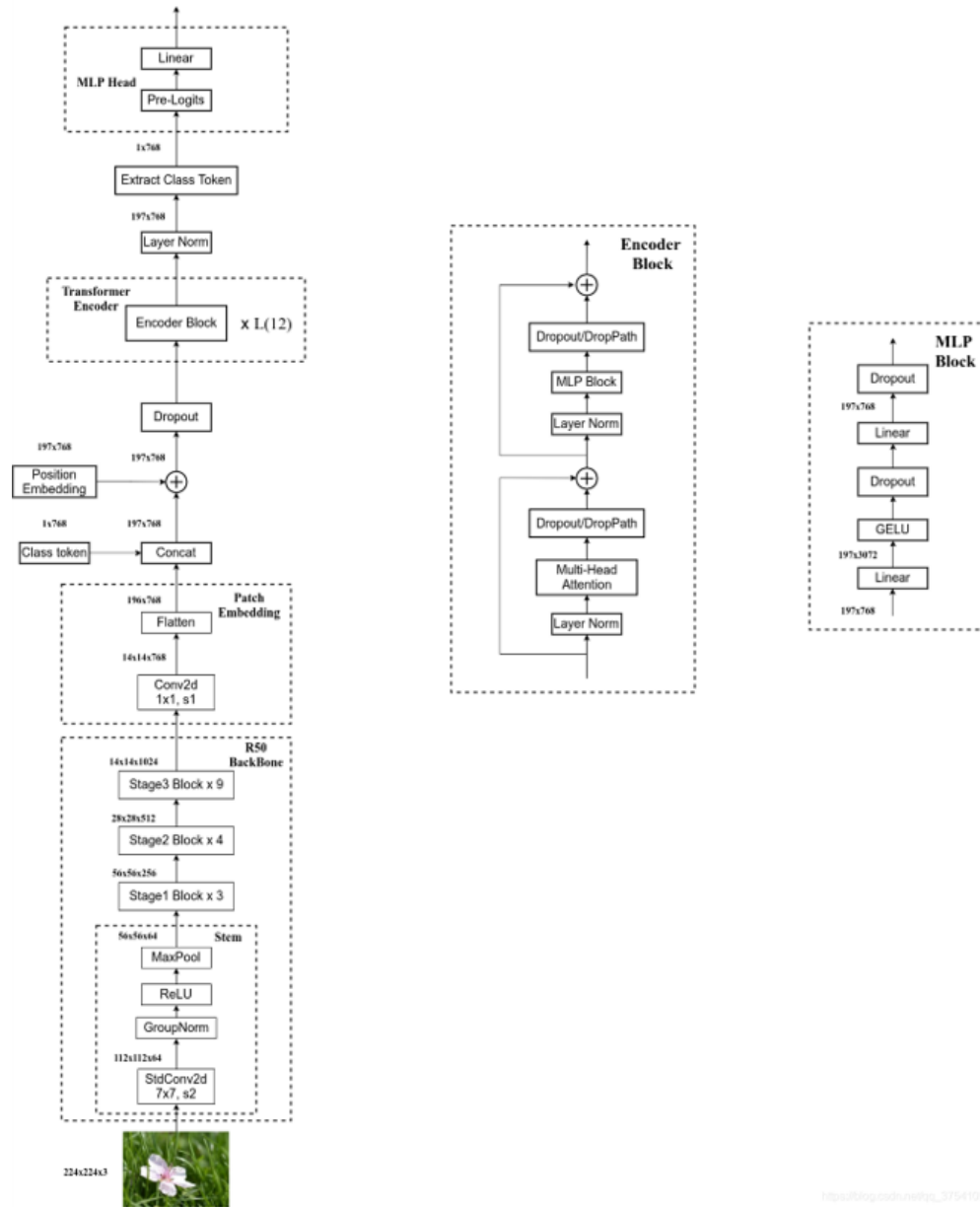


Figure 18: R50+ViT-B.16 hybrid model

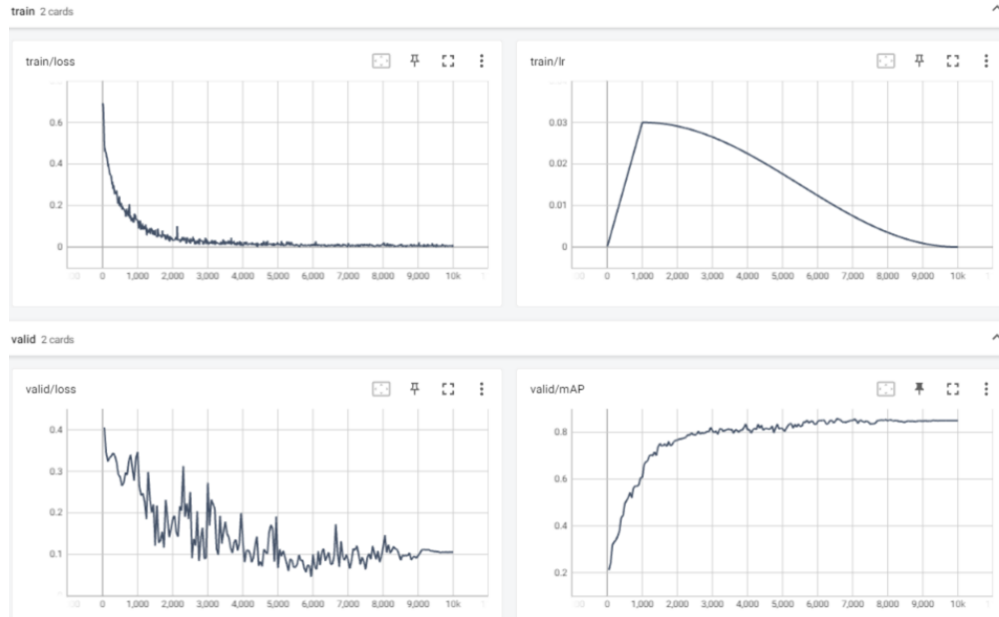


Figure 19: The training process.

### 3.11.1 Method Description

The authors developed a method that localized different surgical instruments in surgical videos with a two-stage model, a detection foundation model based on YOLOv5 [64] to derive the bounding boxes and a classifier based on the ConvNext [27] architecture.

- **Architecture Design:** The authors proposed a two-stage framework by combining two standard architectures YOLOv5 and ConvNext. YOLOv5 was used for the task of object detection. ConvNext, on the other hand, was used for image classification. The training was organized in a way that would reduce the effect of noisy labels.
- **Data Preprocessing:** According to the authors, the dataset posed many challenges due to the following reasons:
  - **Dataset Imbalance:** As per the data exploration done by the authors, the imbalance in the dataset was huge. The videos contained some instruments which appeared thousands of times as compared to the others which appeared only tens of times as shown in Figure 20. The authors balanced the dataset by sampling videos with different frame rates taking into account the types of tools present in each video. They also optimized (minimized) the standard deviation of the frequency of each tool in the resulting dataset.
  - **Presence of banners:** The banners showed the tools used in the surgery, and as proposed by the authors, the removal of the banners was crucial as it could have caused the model to learn the labels from the banners and not actually identify the instruments for their proper classification.
  - **Noisy Labels:** The authors, upon careful inspection of the videos in the dataset, discovered that some tools might never appear in the video even though the label suggested otherwise, which made the labels noisy and the training challenging.
- **Data Augmentation:** Due to the nature of the dataset, where numerous frames were similar, the authors proposed different transformations that could help in training. Different types of augmentations were used for the detection model and the classifier model. For detection, the authors used mosaic augmentation, mixup augmentation, and random perspective transformations. On the other hand, for the classifier, the authors used random image flipping, rotation, and color jittering.

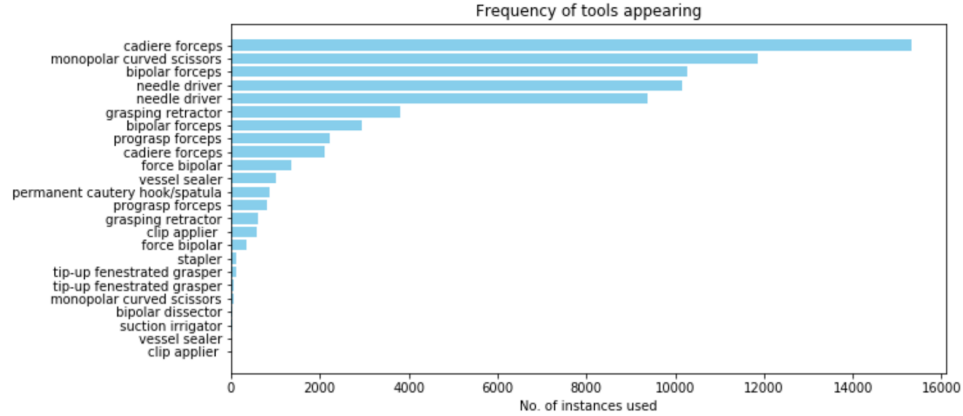


Figure 20: Frequency of each tool across the whole dataset. The graph illustrates the frequent appearance of some tools compared to the other tools. This creates a huge imbalance in the dataset.



Figure 21: Surgical instruments present in Cholec80 Dataset. The tools are similar to the tools present in the challenge dataset.

- Model Input(s): As an end-to-end model, the proposed framework was designed to have a video frame (RGB image) as an input. The frames were obtained by processing the video data provided.
- Model Output(s): For each of the input frames, the framework independently outputs a set of labels for surgical tools present in the respective frame.
- Model Loss Function: The authors used a combination of box regression loss and objectness loss in order to train the localization model and a focal loss as the criterion for the classifier in order to partially mitigate the impact of the huge class imbalance in the dataset.
- Model Pretraining: The authors maintained that pretraining the model on different datasets that had similar characteristics as the provided data would, to some extent, boost the performance of the models. They trained ResNet50 and ConvNext on Cholec 80 [19] and M2CAI [20]. Cholec 80 dataset consists of 80 cholecystectomy surgeries. The labels present are primarily phase and tool presence annotations, where the ground truth for phase annotations is shown in Figure 21 and has been confirmed by a surgeon. On the other hand, the m2cai16-tool-locations dataset contains 15 videos with tool annotations for seven surgical instruments, as shown in Figure 22. The labels are given per frame for 7 classes for each video.

For the task of classification, out of various CNN architectures, ConvNext-Small provided the best results. However, the authors made the following assumptions about the data:



Figure 22: Surgical instruments present in M2CAI Dataset. Some of the tools present are similar to the ones present in the given dataset.

1. They considered and filtered frames where all three instruments were present. They assumed that these frames were sufficient for the task of classification. They also assume that the distribution of surgical tools in these frames would be approximately the same as that in the actual dataset.
2. In the vast majority of frames, the order in which the tools are listed on the label of a clip corresponds to the counter-clockwise order of their positions, starting from the upper left corner and ending with the upper right corner.

Training algorithm: The authors used the localization model Yolov5 pre-trained on a combination of three datasets: EndoVis'15 Instrument Subchallenge Dataset, CholecSeg8k [65] and Endoscopic instrument segmentation with crowdsourced data challenge dataset [66] to detect the surgical tools in a frame with bounding boxes. The bounding boxes were saved as separate images alongside their respective image-level ID number derived from their position relative to the center of the image in an anti-clockwise fashion. The bounding boxes are then assigned the labels from the corresponding video clip (from left to right, depending on the id number of the bounding box). The outputs obtained were a set of predictions for the tools in the frame (Figure 23).

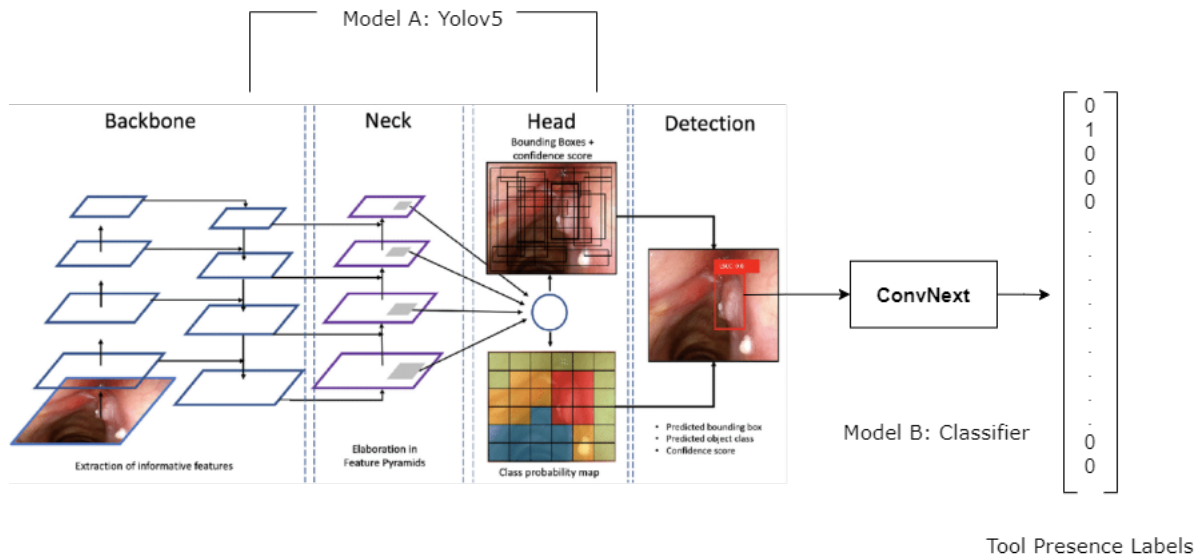


Figure 23: Architecture of the two-tier model used for classification. Images are passed through Yolov5 for generating bounding boxes around the tools. Then they are passed to ConvNext for classification.

### 3.11.2 Model Training

To train the detection model, the authors used a batch size of 128, a learning rate of 0.001, and a total number of epochs of 300. The classifier was using a batch size of 128, a learning rate of 0.0001, and the number of epochs was set to 5 due to the fast convergence of the network.

Given the size of the dataset, the authors used a cluster to run their experiments on a GPU with 2x AMD EPYC 7742 CPUs (128 cores total with 256 threads), 256GB RAM, 4x Nvidia A100 SXM 40G GPUs.

### 3.11.3 Preliminary Performance

The performance of the model during training was quite high with models like ResNet-50 and ConvNext. When pre-trained on the Cholec-80 dataset, ResNet produced a training F1 score of 0.989, while for ConvNext it was 0.985. Moreover, both of them produced around the same F1 scores when trained on the M2CAI dataset. The authors believe that the unrealistically high-performance metrics were due to the similarity across the frames in different surgeries and the usage of the same set of tools for different surgeries with the same background. The validation performance for ConvNext-Small and the proposed two-tier model is shown in Table 12. However, the testing performance for the proposed architecture was around 0.552.

Table 12: Comparison of different models on the performance metrics. Models were pre-trained on Cholec 80 and M2CAI.

MODEL	F1-SCORE	ACCURACY
RESNET-50	0.20	0.10
CONVNEXT-S	<b>0.83</b>	0.39
YOLOV5+CONVNEXT-S	0.75	<b>0.50</b>

## 3.12 University of Tokyo - Team WhiteBox

Team Members: Zhenqiang Li, Yoichi Sato

The authors introduced a network architecture for multi-label surgical tool classification from endoscopic videos. To address the challenge of subtle variance in tool appearance, the network utilizes feature maps from an intermediate layer of ResNet, which retain a higher level of spatial detail. Additionally, the long-tailed class distribution of tools is addressed by employing the asymmetric focal loss in place of the commonly used binary cross-entropy loss.

### 3.12.1 Method Description

The proposed network architecture comprises a feature map extraction module based on the ResNet-18 architecture and a feature post-processing module for multi-label tool classification. A significant challenge in this task is the subtle variance in the appearance of various tools. To address this issue, the network utilizes the feature maps generated by an intermediate layer of the ResNet architecture, as opposed to the final feature obtained after the 2D Average Pooling layer of ResNet. This practice is motivated by the observation that the feature maps obtained at this intermediate stage retain a higher level of spatial detail, thereby enabling the detection of tools with fine variance in appearance. Another critical challenge in this task is the long-tailed class distribution of tools, where the number of samples for the most frequent tool class in the training set is 1149 times that of the least frequent one. To address this imbalance in the training data, the network utilizes the Asymmetric Focal Loss (ASL) [67] in place of the commonly used binary cross-entropy loss as the training loss.

The overall framework for classifying tools' presence in each frame is illustrated in Figure 24. The network utilizes the cascaded first four convolutional blocks of ResNet to extract feature maps for each frame, which have a higher spatial resolution and retain more details in the frame compared to those extracted from the fifth convolutional block or the final average pooling of ResNet. A post-processing module, consisting of an average pool layer (AvgPool) and a Multi-Layer Perceptron (MLP), is utilized to aggregate features in spatial dimensions and conduct feature transformation. The presence probabilities for 14 tools are then predicted on each frame by feeding the post-processed feature into a fully-connected layer (FC) and a Sigmoid activation layer.

The network is trained via asymmetric focal loss (ASL) to overcome the long-tailed class distributions in the training dataset. ASL adapts focal loss for the multi-label classification task by decoupling the focusing levels of the positive and negative samples. Given  $K$  labels, the network predicts one probability per label,



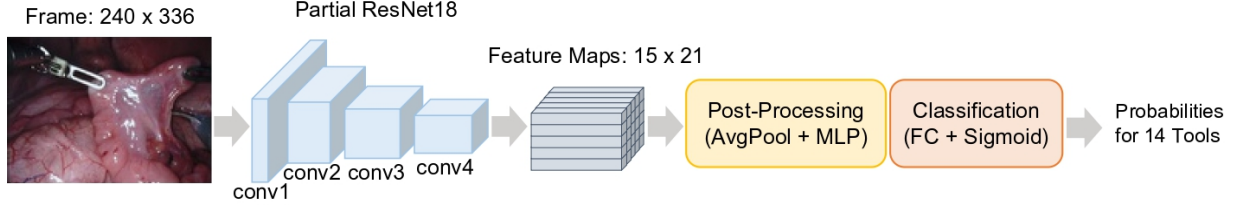


Figure 24: The tool presence classification framework used by WhiteBox team.

$p_k$ , whose ground truth is denoted by  $y_k$ . The total classification loss  $L_{total}$  is obtained by aggregating the binary loss from  $K$  labels as  $L_{total} = \sum_{k=1}^K -y_k L_+(p_k) - (1 - y_k) L_-(p_k)$ . The positive and negative loss parts can be formed as follows by following the focal loss:

$$\begin{cases} L_+ = (1 - p)^\gamma \log(p), \\ L_- = p^\gamma \log(1 - p), \end{cases}$$

where  $p$  is one predicted probability. ASL incorporates two key modifications to the loss in order to improve the multi-label training effect. First, ASL assigns distinct weights, denoted as  $\gamma_+$  and  $\gamma_-$ , to the positive and negative loss parts, respectively. By emphasizing the contribution of positive samples through setting  $\gamma_- > \gamma_+$ , ASL ensures that the network is able to learn meaningful features from positive but infrequent samples. Additionally, in order to reduce the ratio of very easy negative samples on the overall loss, ASL fully discards negative samples when their probability is very low by performing the hard thresholding as  $p_m = \max(p - m, 0)$ . Here  $m \geq 0$  is a tunable hyperparameter for the probability margin. In general, ASL is defined as follows:

$$ASL = \begin{cases} L_+ = (1 - p)^{\gamma_+} \log(p) \\ L_- = (p_m)^{\gamma_-} \log(1 - p_m). \end{cases}$$

### 3.12.2 Implementation Details

During the training phase of the network, the video frames were resized to a height of 270 and a width of 480. Subsequently, the upper-middle regions (shaped in  $240 \times 336$ ) of the resized frames were cropped as input to the network. This cropping process removed the black regions present on both sides and the text labels located at the bottom of the frames. Each training sample for one video was formed by splitting it into 32 segments and randomly sampling one frame from each segment. At the network test phase, the continuous regions with pixel values less than 1, which represented the black background, were first identified and removed from the frames. The remained foreground was then resized to  $270 \times 336$ , from which the upper  $240 \times 336$  regions were cropped as input to the network. All frames of a video were taken as input for making predictions at the test phase. The input RGB frames were normalized using the means of (0.432, 0.395, 0.376) and the standard deviations of (0.228, 0.221, 0.217). The network outputted the existence probabilities of all 14 tools, from which the first 3 classes having probabilities larger than 0.5 were selected as the predicted tool labels.

The framework employed the first four convolutional blocks of a ResNet-18 model pre-trained on ImageNet as the feature extractor. To preserve the high spatial resolution of the output feature maps, the max pooling layer following the first convolutional block is eliminated. The resulting feature maps have a spatial shape of  $15 \times 21$  and 256 channels for a  $336 \times 240$  frame. The MLP for post-processing preserves the feature channel number at 256. These features are finally fed through a linear transformation network and a Sigmoid activation layer to predict frame-wise tool existence probabilities.

The parameters of all components were trained in an end-to-end manner using a Stochastic Gradient Descent (SGD) optimization algorithm for a total of 60 epochs. The learning rate was initially established at 0.01 and decreased by a factor of 10 after the 40th epoch. The training process was conducted using an Nvidia A100-SXM4-40GB GPU, with a batch size of 18. Additionally, the weights for the positive and negative samples in the Asymmetric Focal Loss (ASL) were set as  $\gamma_+ = 1.0$  and  $\gamma_- = 4.0$ , respectively. Furthermore, a probability margin of  $m = 0.05$  was employed to constrain the easy negative samples.

### 3.13 University of Strasbourg - Team CAMMA

Team Members: Chinedu Nwoye, Luca Sestini, and Nicolas Padoy.

#### 3.13.1 Method Description

To detect surgical tools from videos acquired from Da Vinci robotic system, a spatial attention network (SANet) was proposed. This was motivated by the characteristics and constraints of the provided dataset: (1) the videos were annotated with binary presence labels from the Da Vinci user interface (UI) - in this case, a set of tool labels was fixed for a video with a high level of inconsistency when considered at a frame level, (2) utilizing the UI information was not allowed for the SurgToolLoc challenge and would also be blurred for the test videos, and (3) the test labels would be frame-based, more accurate, and thus, not a fair representation of the provided training videos and labels. Taking these limitations into consideration, the SANet model was designed to discover more useful features that could represent the tools' presence and yet with some level of tolerance to the noisy ground truths.

The model and its implementation details are summarized as follows:

- **Architecture design:** The SANet consists of 3 modules as shown in Figure 25: (1) a ResNet-18 [45] backbone to extract spatial features from the input images, (2) a spatial attention module, consisting of 8 layers of a self-attention unit [68], to highlight the discriminating regions of the input features for the tools with each feature channel constrained by designed to focus on a distinct tool class, and (3) a global pooling-based classifier [69] to transform the attention features to a vector of class-wise probabilities for the 14 tool classes considered in the dataset.
- **Data processing:** The images were cropped to eliminate UI sections before being resized to a  $360 \times 640$  spatial dimension because the video frames contain a sort of tool information from the Da Vinci UI that would not be available during testing.
- **Data augmentation:** The input images were augmented using color jittering, flipping, random rotation, and random adjustment of brightness/contrast.
- **Model input:** During training, the model received pre-processed and augmented inputs, while during inference, it received solely pre-processed inputs.
- **Model outputs:** The output was a vector representing the log probability of each tool category appearing in the image. The output attention maps also included location-based activations for tool instances, which helped localize the tools in a weakly-supervised scenario.
- **Model loss function:** The model was trained using weighted sigmoid cross entropy loss. The class weights were computed by median-weighted inverse frequency given in [69].
- **Model pre-training:** The ResNet-18 backbone was pretrained on ImageNet [21].
- **Post-processing:** The output vector of the model was converted to binary labels at a threshold of 0.5 and the positive class identities were mapped to the tool labels.

Using its ResNet-18 backbone, the SANet model extracts spatial features from an input image. The spatial self-attention module highlights the feature regions that belong to the tools while suppressing those that belong to the background. The classifier pools the maximal activations of the feature channels into a vector of logits for each tool type, using the same methodology as in [70] and then transforms the logits to presence probability scores by a sigmoid operation. Casting the values to binary at a threshold of 0.5 yields the desired result.

#### 3.13.2 Model Training

The provided dataset was split into train, validation, and test sets for the experiment. Training elapsed after 30 epochs using a batch size of 30 frames randomly composed from 3 video clips extracted at 1 fps. Model weight optimization was performed using a Stochastic Gradient Descent (SGD) optimizer (Momentum

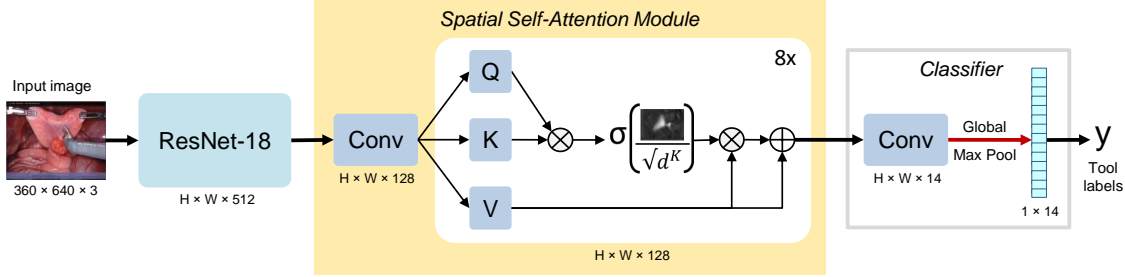


Figure 25: Architecture of the spatial attention network (SANet) for surgical tool presence detection

$\rho = 0.9$ ) with an initial learning rate ( $\lambda = 7e^{-3}$ ), decayed by a factor ( $\eta = 1e^{-4}$ ) and regularized by an  $L_2$  norm. Optimal hyper-parameters were selected using the validation set.

The presented SANet model was trained on 4x Quadro RTX 6000 24GiB GPU provided by HPC Unistra Mesocenter managed by the University of Strasbourg, France.

## 4 Results

The team evaluations for the challenge were performed on a private, hidden test set containing individual files of surgical videos at 1 FPS. The results were generated through the Grand Challenge automated algorithm submission and evaluation system. Below we present a summary of the challenge results.

### 4.1 Category 1: Surgical tool presence detection

For Category 1, the performance of surgical tool presence detection was evaluated with the mean F1-score [71] across all tools. Overall, the teams performed well in this category with some of them obtaining F1-scores above 0.7 (Table 13). It is important to notice that the presented F1-scores take into consideration data imbalance: the scores are weighted based on how often each tool is present in the test data. This was an important consideration because some tools did appear much more often than others in this data set.

Table 13: Results for Category 1

Team	Avg. F1-score
HRI.MV	0.7485
HKMV	0.72
NVIDIA	0.7055
ANL-Surg	0.6691
HVRL	0.6605
SK	0.643
TeamZERO	0.6299
VANDY-UISE	0.6206
UKE	0.6203
Gatech	0.5986
ITeM	0.5978
MM	0.5637
BioMedIA	0.5521

### 4.2 Category 2: Surgical tool localization and classification

For this category the performance of surgical tool localization and classification was evaluated with the standard COCO dataset evaluation metric [72], i.e. the mean average precision (mAP) of intersection over

Table 14: Results for Category 2

Team	mAP
HRLMV	0.4077
HKMV	0.3726
NVIDIA	0.3058
ANL-Surg	0.0961
Gatech	0.0686
SK	0.0247
VANDY-VISE	0.0003
HVRL	0
ITeM	0

union (IoU), discretized with values 0.5 : 0.05 : 0.95 at 1 FPS. This challenge proved to be very demanding for most teams. Only the top 3 teams were able to achieve a reasonable performance of above 0.3 mAP on the test set. The remainder of the teams struggled with detecting bounding boxes accurately and could only achieve mAP values between 0 and 0.1 (Table 14).

Unsurprisingly, teams that performed well in Category 2 also performed well in Category 1. Interestingly, lower performance in Category 2 could still translate to reasonable performance in Category 1. This indicates that detection models may be learning image features that do not help with localization. Critically, the method that distinguishes higher from lower-performing results in Category 2 is pre-training on some data sets with ground truth tool segmentation labels. This may suggest that “nudging” the model weights to some portions of the weight-space that are informed by tool segmentation, helping learn features that are more relevant to localization.

## 5 Discussion

Alternatives to fully supervised learning, such as self-supervision and weak supervision, continue to advance in the areas of object classification, detection, and localization. This is particularly impactful in surgical data science since large volumes of data can be exploited if noisy or weak labels can be utilized. Our SurgToolLoc 2022 EndoVis challenge provided the community with just such a dataset. With all the trappings of a large, real-world dataset (e.g. variability, imbalanced classes, noisy and weak labels), teams could explore how different model architectures and training strategies could solve a relevant surgical task.

In total, there were 13 complete submissions in Category 1 and nine complete submissions in Category 2. Team reports were included to provide a comprehensive view of the approaches taken. Teams performed relatively well in Category 1 but struggled in Category 2. Good performance in Category 1 generally translated to relatively good performance in Category 2. This was perhaps not surprising since discovering an accurate and robust representation of the tool presence, at least conceptually, seems like a prerequisite for localizing these same tools.

For both categories 1 and 2, supplementing training data with publicly available surgical data (e.g. Cholec80), or building off of previously trained backbones (e.g. resnet) proved to be key in getting high-performing models. Specifically, five out of the 13 teams used a clinical dataset to pre-train the model. For Category 1, three out of the top five teams used the EndoVis instrument segmentation dataset to pre-train the model, including HRI-MV, HKMV, and ANL-Surg. Similarly for category 2, two out of the top three teams used the same dataset, including HRI-MV and HKMV. For Category 2, the use of class activation maps was crucial but only proved moderately successful. On the whole, the challenge was difficult and the proposed tasks remain largely unsolved.

Performance in Category 2 was clearly worse than that of Category 1, but also poor by conventional standards. This was not surprising as only noisy, weak labels were available for training. All other things being equal, we assume supervised training would improve performance on this task. By how much is not clear. It could be that performance of these weakly supervised models would be viewed more favorably in light of the limits of similar models trained with strong labels. This would have important implications given

the difficulties and resources required in obtaining strong labels. We plan to pursue this question in future work.

The training data used in this study will be made publicly available. This decision was made to assist efforts on problems similar to the one pursued here, but also for the community’s broader efforts in surgical data science. There are a host of topics that could be explored with this data. For example, surgical gesture and activity recognition, and tool-tissue interaction are areas of study that this data set can speak to, albeit with various annotation efforts. Similarly, automated, objective skill assessment is an important area that could potentially benefit from this and similar data sets. We hope that this data set can contribute to many future advances.

## 6 Conclusion

In this challenge, we encouraged the surgical data science community to tackle the problem of automatically detecting and tracking surgical instruments in endoscopic videos. This had to be accomplished by leveraging only tool presence data, as this data is readily available in robotic-assisted surgery. For category 1, designed to classify tools present in each surgical frame, the participating teams developed algorithms that performed well. For category 2, classifying and detecting the spatial locations of surgical instruments, the algorithms performed relatively poorly. The models used by the teams represent many state-of-the-art classifier algorithms. While these models perform well on natural and conventional image data sets, they failed to exhibit similar performance on these surgical videos. We can only speculate as to the reasons for these shortcomings. For instance, it could be due to the noisy labels; it could be that these surgical images represent an entirely different distribution of data that is more difficult to categorize; it could be that this problem has exposed the limitations of these algorithms; or, it could be that these algorithms simply require more training data. While the lack of sufficient training data is the usual culprit for poor performance, it is worth noting once more that we believe this is the largest publicly available surgical data set to date. Regardless of where the models fell short, it is clear that this problem has not been solved. As we believe this is an important problem for the surgical data science community at large, we will continue to encourage work in this area by releasing this data set to the public, as well as our continued effort to host similar ML challenges.

## 7 Acknowledgements

Work done by the CAMMA team was supported by French state funds managed within the Plan Investissements d’Avenir by the ANR under references: National AI Chair AI4ORSafety [ANR-20-CHIA-0029-01], Labex CAMI [ANR-11-LABX-0004], DeepSurg [ANR-16-CE33-0009], IHU Strasbourg [ANR-10-IAHU-02] and by BPI France under references: project CONDOR, project 5G-OR.

Work done by the ITeM team was supported by the German Federal Ministry of Research and Education (BMBF) under grants CoHMed/DigiMedOP grant no. 13FH5I05IA, CoHMed/PersonaMed-A grant no. 13FH5I06IA, and CoHMed/PersonaMed-B grant no. 13FH5I09IA.

## References

- [1] Michael A Mederos, R Lorie Jacob, Rachel Ward, Rivfka Shenoy, Melinda M Gibbons, Mark D Girgis, Devan Kansagara, Denise Hynes, Paul G Shekelle, and Karli Kondo. Trends in robot-assisted procedures for general surgery in the veterans health administration. *Journal of Surgical Research*, 279:788–795, 2022.
- [2] Emily A Grimsley, Tara M Barry, Haroon Janjua, Emanuel Eguia, Christopher DuCoin, and Paul C Kuo. Exploring the paradigm of robotic surgery and its contribution to the growth of surgical volume. *Surgery Open Science*, 10:36–42, 2022.
- [3] Lena Maier-Hein, Matthias Eisenmann, Duygu Sarikaya, Keno März, Toby Collins, Anand Malpani, Johannes Fallert, Hubertus Feussner, Stamatia Giannarou, Pietro Mascagni, et al. Surgical data science—from concepts toward clinical translation. *Medical image analysis*, 76:102306, 2022.
- [4] S Swaroop Vedula and Gregory D Hager. Surgical data science: the new knowledge domain. *Innovative surgical sciences*, 2(3):109–121, 2017.
- [5] Sonia Guerin, Arnaud Huaultmé, Vincent Lavoue, Pierre Jannin, and Krystel Nyangoh Timoh. Review of automated performance metrics to assess surgical technical skills in robot-assisted laparoscopy. *Surgical Endoscopy*, pages 1–18, 2022.
- [6] Francisco Luongo, Ryan Hakim, Jessica H Nguyen, Animashree Anandkumar, and Andrew J Hung. Deep learning-based computer vision to recognize and classify suturing gestures in robot-assisted surgery. *Surgery*, 169(5):1240–1244, 2021.
- [7] Andrew J Hung, Jian Chen, Saum Ghodoussipour, Paul J Oh, Zequn Liu, Jessica Nguyen, Sanjay Purushotham, Inderbir S Gill, and Yan Liu. A deep-learning model using automated performance metrics and clinical features to predict urinary continence recovery after robot-assisted radical prostatectomy. *BJU international*, 124(3):487–495, 2019.
- [8] Kristen C Brown, Kiran D Bhattacharyya, Sue Kulason, Aneeq Zia, and Anthony Jarc. How to bring surgery to the next level: interpretable skills assessment in robotic-assisted surgery. *Visceral medicine*, 36(6):463–470, 2020.
- [9] Aneeq Zia and Irfan Essa. Automated surgical skill assessment in rmis training. *International journal of computer assisted radiology and surgery*, 13(5):731–739, 2018.
- [10] Aneeq Zia, Chi Zhang, Xiaobin Xiong, and Anthony M Jarc. Temporal clustering of surgical activities in robot-assisted surgery. *International journal of computer assisted radiology and surgery*, 12(7):1171–1178, 2017.
- [11] Aneeq Zia, Liheng Guo, Linlin Zhou, Irfan Essa, and Anthony Jarc. Novel evaluation of surgical activity recognition models using task-based efficiency metrics. *International journal of computer assisted radiology and surgery*, 14(12):2155–2163, 2019.
- [12] Aneeq Zia, Andrew Hung, Irfan Essa, and Anthony Jarc. Surgical activity recognition in robot-assisted radical prostatectomy using deep learning. In *International Conference on Medical Image Computing and Computer-Assisted Intervention*, pages 273–280. Springer, 2018.
- [13] Matthias Eisenmann, Annika Reinke, Vivienn Weru, Minu Dietlinde Tizabi, Fabian Isensee, Tim J Adler, Patrick Godau, Veronika Cheplygina, Michal Kozubek, Sharib Ali, et al. Biomedical image analysis competitions: The state of current participation practice. *arXiv preprint arXiv:2212.08568*, 2022.
- [14] Aneeq Zia, Kiran Bhattacharyya, Xi Liu, Ziheng Wang, Satoshi Kondo, Emanuele Colleoni, Beatrice van Amsterdam, Razeen Hussain, Raabid Hussain, Lena Maier-Hein, et al. Surgical visual domain adaptation: results from the miccai 2020 surgvisdom challenge. *arXiv preprint arXiv:2102.13644*, 2021.

- [15] Zixu Zhao, Yueming Jin, Xiaojie Gao, Qi Dou, and Pheng-Ann Heng. Learning motion flows for semi-supervised instrument segmentation from robotic surgical video. In *Medical Image Computing and Computer Assisted Intervention–MICCAI 2020: 23rd International Conference, Lima, Peru, October 4–8, 2020, Proceedings, Part III 23*, pages 679–689. Springer, 2020.
- [16] Aneeq Zia, Kiran Bhattacharyya, Xi Liu, Ziheng Wang, Max Berniker, Satoshi Kondo, Emanuele Colleoni, Dimitris Psychogios, Yueming Jin, Jinfan Zhou, et al. Objective surgical skills assessment and tool localization: Results from the miccai 2021 simsurgskill challenge. *arXiv preprint arXiv:2212.04448*, 2022.
- [17] Max Allan, Jonathan Mcleod, Congcong Wang, Jean Claude Rosenthal, Zhenglei Hu, Niklas Gard, Peter Eisert, Ke Xue Fu, Trevor Zeffiro, Wenyao Xia, et al. Stereo correspondence and reconstruction of endoscopic data challenge. *arXiv preprint arXiv:2101.01133*, 2021.
- [18] Max Allan, Satoshi Kondo, Sebastian Bodenstedt, Stefan Leger, Rahim Kadkhodamohammadi, Imanol Luengo, Felix Fuentes, Evangello Flouty, Ahmed Mohammed, Marius Pedersen, Avinash Kori, Varghese Alex, Ganapathy Krishnamurthi, David Rauber, Robert Mendel, Christoph Palm, Sophia Bano, Guinther Saibro, Chi-Sheng Shih, Hsun-An Chiang, Juntang Zhuang, Junlin Yang, Vladimir Iglovikov, Anton Dobrenkii, Madhu Reddiboina, Anubhav Reddy, Xingtong Liu, Cong Gao, Mathias Unberath, Myeonghyeon Kim, Chanh Kim, Chaewon Kim, Hyejin Kim, Gyeongmin Lee, Ihsan Ullah, Miguel Luna, Sang Hyun Park, Mahdi Azizian, Danail Stoyanov, Lena Maier-Hein, and Stefanie Speidel. 2018 robotic scene segmentation challenge, 2020.
- [19] Andru P Twinanda, Sherif Shehata, Didier Mutter, Jacques Marescaux, Michel De Mathelin, and Nicolas Padoy. Endonet: a deep architecture for recognition tasks on laparoscopic videos. *IEEE transactions on medical imaging*, 36(1):86–97, 2016.
- [20] Amy Jin, Serena Yeung, Jeffrey Jopling, Jonathan Krause, Dan Azagury, Arnold Milstein, and Li Fei-Fei. Tool detection and operative skill assessment in surgical videos using region-based convolutional neural networks. In *2018 IEEE winter conference on applications of computer vision (WACV)*, pages 691–699. IEEE, 2018.
- [21] Olga Russakovsky, Jia Deng, Hao Su, Jonathan Krause, Sanjeev Satheesh, Sean Ma, Zhiheng Huang, Andrej Karpathy, Aditya Khosla, Michael Bernstein, et al. Imagenet large scale visual recognition challenge. *International journal of computer vision*, 115(3):211–252, 2015.
- [22] Yinda Xu, Zeyu Wang, Zuoxin Li, Ye Yuan, and Gang Yu. Siamfc++: Towards robust and accurate visual tracking with target estimation guidelines. In *Proceedings of the AAAI conference on artificial intelligence*, volume 34, pages 12549–12556, 2020.
- [23] Zhaowei Cai and Nuno Vasconcelos. Cascade r-cnn: Delving into high quality object detection. In *Proceedings of the IEEE conference on computer vision and pattern recognition*, pages 6154–6162, 2018.
- [24] Max Allan, Alex Shvets, Thomas Kurmann, Zichen Zhang, Rahul Duggal, Yun-Hsuan Su, Nicola Rieke, Iro Laina, Niveditha Kalavakonda, Sebastian Bodenstedt, et al. 2017 robotic instrument segmentation challenge. *arXiv preprint arXiv:1902.06426*, 2019.
- [25] Max Allan, Satoshi Kondo, Sebastian Bodenstedt, Stefan Leger, Rahim Kadkhodamohammadi, Imanol Luengo, Felix Fuentes, Evangello Flouty, Ahmed Mohammed, Marius Pedersen, et al. 2018 robotic scene segmentation challenge. *arXiv preprint arXiv:2001.11190*, 2020.
- [26] Alexey A Shvets, Alexander Rakhlin, Alexandr A Kalinin, and Vladimir I Iglovikov. Automatic instrument segmentation in robot-assisted surgery using deep learning. In *2018 17th IEEE international conference on machine learning and applications (ICMLA)*, pages 624–628. IEEE, 2018.
- [27] Zhuang Liu, Hanzi Mao, Chao-Yuan Wu, Christoph Feichtenhofer, Trevor Darrell, and Saining Xie. A convnet for the 2020s. In *Proceedings of the IEEE/CVF Conference on Computer Vision and Pattern Recognition*, pages 11976–11986, 2022.

- [28] Mingxing Tan and Quoc Le. Efficientnet: Rethinking model scaling for convolutional neural networks. In *International conference on machine learning*, pages 6105–6114. PMLR, 2019.
- [29] Ramprasaath R Selvaraju, Michael Cogswell, Abhishek Das, Ramakrishna Vedantam, Devi Parikh, and Dhruv Batra. Grad-cam: Visual explanations from deep networks via gradient-based localization. In *Proceedings of the IEEE international conference on computer vision*, pages 618–626, 2017.
- [30] Glenn Jocher. YOLOv5 by Ultralytics, 5 2020.
- [31] Puzuo Wang and Wei Yao. Weakly supervised pseudo-label assisted learning for als point cloud semantic segmentation. *arXiv preprint arXiv:2105.01919*, 2021.
- [32] Max Allan, Satoshi Kondo, Sebastian Bodenstedt, Stefan Leger, Rahim Kadkhodamohammadi, Imanol Luengo, Felix Fuentes, Evangello Flouty, Ahmed Mohammed, Marius Pedersen, Avinash Kori, Varghese Alex, Ganapathy Krishnamurthi, David Rauber, Robert Mendel, Christoph Palm, Sophia Bano, Guinther Saibro, Chi-Sheng Shih, Hsun-An Chiang, Juntang Zhuang, Junlin Yang, Vladimir Iglovikov, Anton Dobrenkii, Madhu Reddiboina, Anubhav Reddy, Xingtong Liu, Cong Gao, Mathias Unberath, Myeonghyeon Kim, Chanho Kim, Chaewon Kim, Hyejin Kim, Gyeongmin Lee, Ihsan Ullah, Miguel Luna, Sang Hyun Park, Mahdi Azizian, Danail Stoyanov, Lena Maier-Hein, and Stefanie Speidel. 2018 robotic scene segmentation challenge, 2020.
- [33] Max Allan, Alex Shvets, Thomas Kurmann, Zichen Zhang, Rahul Duggal, Yun-Hsuan Su, Nicola Rieke, Iro Laina, Niveditha Kalavakonda, Sebastian Bodenstedt, Luis Herrera, Wenqi Li, Vladimir Iglovikov, Huoling Luo, Jian Yang, Danail Stoyanov, Lena Maier-Hein, Stefanie Speidel, and Mahdi Azizian. 2017 robotic instrument segmentation challenge, 2019.
- [34] Jeremy Howard and Sylvain Gugger. Fastai: A layered API for deep learning. *Information*, 11(2):108, feb 2020.
- [35] Yuxin Wu, Alexander Kirillov, Francisco Massa, Wan-Yen Lo, and Ross Girshick. Detectron2, 2019.
- [36] Ryo Fujii, Ryo Hachiuma, Hiroki Kajita, and Hideo Saito. Surgical tool detection in open surgery videos. *Applied Sciences*, 12(20), 2022.
- [37] Ze Liu, Han Hu, Yutong Lin, Zhuliang Yao, Zhenda Xie, Yixuan Wei, Jia Ning, Yue Cao, Zheng Zhang, Li Dong, Furu Wei, and Baining Guo. Swin transformer v2: Scaling up capacity and resolution. In *CVPR*, pages 12009–12019, June 2022.
- [38] Mingxing Tan and Quoc Le. Efficientnetv2: Smaller models and faster training. In *ICML*, 2021.
- [39] Saining Xie, Ross B. Girshick, Piotr Dollár, Zhuowen Tu, and Kaiming He. Aggregated residual transformations for deep neural networks. *CoRR*, abs/1611.05431, 2016.
- [40] Ross Wightman. Pytorch image models, 2019.
- [41] Aditya Chattopadhyay, Anirban Sarkar, Prantik Howlader, and Vineeth N Balasubramanian. Grad-cam++: Generalized gradient-based visual explanations for deep convolutional networks. In *WACV*, 2018.
- [42] Jia Deng, Wei Dong, Richard Socher, Li-Jia Li, Kai Li, and Li Fei-Fei. Imagenet: A large-scale hierarchical image database. In *CVPR*, 2009.
- [43] Jun Wei, Qin Wang, Zhen Li, Sheng Wang, S Kevin Zhou, and Shuguang Cui. Shallow feature matters for weakly supervised object localization. In *Proceedings of the IEEE/CVF Conference on Computer Vision and Pattern Recognition*, pages 5993–6001, 2021.
- [44] Shilong Liu, Lei Zhang, Xiao Yang, Hang Su, and Jun Zhu. Query2label: A simple transformer way to multi-label classification. *arXiv preprint arXiv:2107.10834*, 2021.



- [45] Kaiming He, Xiangyu Zhang, Shaoqing Ren, and Jian Sun. Deep residual learning for image recognition. In *Proceedings of the IEEE conference on computer vision and pattern recognition*, pages 770–778, 2016.
- [46] Emanuel Ben-Baruch, Tal Ridnik, Nadav Zamir, Asaf Noy, Itamar Friedman, Matan Protter, and Lih Zelnik-Manor. Asymmetric loss for multi-label classification. *arXiv preprint arXiv:2009.14119*, 2020.
- [47] Gary Bradski. The opencv library. *Dr. Dobb’s Journal: Software Tools for the Professional Programmer*, 25(11):120–123, 2000.
- [48] Mathilde Caron, Hugo Touvron, Ishan Misra, et al. Emerging Properties in Self-Supervised Vision Transformers. In *ICCV*, 2021.
- [49] Jinghao Zhou, Chen Wei, Huiyu Wang, et al. iBOT: Image BERT Pre-Training with Online Tokenizer. *ICLR*, 2022.
- [50] Max Allan, Alex Shvets, Thomas Kurmann, et al. 2017 robotic instrument segmentation challenge. *arXiv preprint arXiv:1902.06426*, 2019.
- [51] Andru P Twinanda, Sherif Shehata, Didier Mutter, Jacques Marescaux, Michel De Mathelin, and Nicolas Padoy. Endonet: a deep architecture for recognition tasks on laparoscopic videos. *IEEE transactions on medical imaging*, 36(1):86–97, 2016.
- [52] Tamer Abdalbaki Alshirbaji, Nour Aldeen Jalal, Paul D Docherty, Thomas Neumuth, and Knut Möller. A deep learning spatial-temporal framework for detecting surgical tools in laparoscopic videos. *Biomedical Signal Processing and Control*, 68:102801, 2021.
- [53] Thibaut Durand, Taylor Mordan, Nicolas Thome, and Matthieu Cord. Wildcat: Weakly supervised learning of deep convnets for image classification, pointwise localization and segmentation. In *Proceedings of the IEEE Conference on Computer Vision and Pattern Recognition*, pages 642–651, 2017.
- [54] Armine Vardazaryan, Didier Mutter, Jacques Marescaux, and Nicolas Padoy. Weakly-supervised learning for tool localization in laparoscopic videos. In *Intravascular Imaging and Computer Assisted Stenting and Large-Scale Annotation of Biomedical Data and Expert Label Synthesis*, pages 169–179. Springer, 2018.
- [55] Chinedu Innocent Nwoye, Didier Mutter, Jacques Marescaux, and Nicolas Padoy. Weakly supervised convolutional LSTM approach for tool tracking in laparoscopic videos. *International journal of computer assisted radiology and surgery*, 14(6):1059–1067, 2019.
- [56] Kaiming He, Xiangyu Zhang, Shaoqing Ren, and Jian Sun. Deep residual learning for image recognition. In *Proceedings of the IEEE Conference on Computer Vision and Pattern Recognition*, pages 770–778, 2016.
- [57] Jie Hu, Li Shen, and Gang Sun. Squeeze-and-excitation networks. In *Proceedings of the IEEE Conference on Computer Vision and Pattern Recognition*, pages 7132–7141, 2018.
- [58] T. Abdalbaki Alshirbaji, Nour A. Jalal, Paul D. Docherty, P. T. Neumuth, and Knut Möller. Improving the Generalisability of Deep CNNs by Combining Multi-stage Features for Surgical Tool Classification. In *2022 44th Annual International Conference of the IEEE Engineering in Medicine & Biology Society (EMBC)*, pages 533–536. IEEE, 2022.
- [59] Tamer Abdalbaki Alshirbaji, Nour Aldeen Jalal, and Knut Möller. Surgical tool classification in laparoscopic videos using convolutional neural network. *Current Directions in Biomedical Engineering*, 4(1):407–410, 2018.
- [60] et al. Dosovitskiy, Alexey. An image is worth 16x16 words: Transformers for image recognition at scale. *arXiv preprint*, 2020.
- [61] DeVries Terrance, and Graham W. Taylor. Improved regularization of convolutional neural networks with cutout. *arXiv preprint*.

- [62] et al. Cubuk, Ekin D. Randaugment: Practical automated data augmentation with a reduced search space. *arXiv e-prints*, 2019.
- [63] et al. Ridnik, Tal. Asymmetric loss for multi-label classification. *IEEE/CVF International Conference on Computer Vision*, 2021.
- [64] Alexey Bochkovskiy, Chien-Yao Wang, and Hong-Yuan Mark Liao. Yolov4: Optimal speed and accuracy of object detection. *arXiv preprint arXiv:2004.10934*, 2020.
- [65] W-Y Hong, C-L Kao, Y-H Kuo, J-R Wang, W-L Chang, and C-S Shih. Cholecseg8k: a semantic segmentation dataset for laparoscopic cholecystectomy based on cholec80. *arXiv preprint arXiv:2012.12453*, 2020.
- [66] Lena Maier-Hein, Sven Mersmann, Daniel Kondermann, Sebastian Bodenstedt, Alexandro Sanchez, Christian Stock, Hannes Gotz Kenngott, Mathias Eisenmann, and Stefanie Speidel. Can masses of non-experts train highly accurate image classifiers? In *International conference on medical image computing and computer-assisted intervention*, pages 438–445. Springer, 2014.
- [67] Tal Ridnik, Emanuel Ben-Baruch, Nadav Zamir, Asaf Noy, Itamar Friedman, Matan Protter, and Lih Zelnik-Manor. Asymmetric loss for multi-label classification. In *Proceedings of the IEEE/CVF International Conference on Computer Vision*, pages 82–91, 2021.
- [68] Ashish Vaswani, Noam Shazeer, Niki Parmar, Jakob Uszkoreit, Llion Jones, Aidan N Gomez, Łukasz Kaiser, and Illia Polosukhin. Attention is all you need. *Advances in neural information processing systems*, 30, 2017.
- [69] Chinedu Innocent Nwoye, Didier Mutter, Jacques Marescaux, and Nicolas Padoy. Weakly supervised convolutional lstm approach for tool tracking in laparoscopic videos. *International journal of computer assisted radiology and surgery*, 14:1059–1067, 2019.
- [70] Chinedu Innocent Nwoye, Tong Yu, Cristians Gonzalez, Barbara Seeliger, Pietro Mascagni, Didier Mutter, Jacques Marescaux, and Nicolas Padoy. Rendezvous: Attention mechanisms for the recognition of surgical action triplets in endoscopic videos. *Medical Image Analysis*, 78:102433, 2022.
- [71] F. Pedregosa, G. Varoquaux, A. Gramfort, V. Michel, B. Thirion, O. Grisel, M. Blondel, P. Prettenhofer, R. Weiss, V. Dubourg, J. Vanderplas, A. Passos, D. Cournapeau, M. Brucher, M. Perrot, and E. Duchesnay. Scikit-learn: Machine learning in Python. *Journal of Machine Learning Research*, 12:2825–2830, 2011.
- [72] Tsung-Yi Lin, Michael Maire, Serge Belongie, James Hays, Pietro Perona, Deva Ramanan, Piotr Dollár, and C Lawrence Zitnick. Microsoft coco: Common objects in context. In *European conference on computer vision*, pages 740–755. Springer, 2014.